# Cell cycle checkpoint activity in the malaria parasite *Plasmodium falciparum*

**Monique K. Johnson[1], Juliana Naldoni[1], William H. Lewis[2], Ross F. Waller[2], Catherine J. Merrick[1*]**

[1] Department of Pathology, University of Cambridge, Tennis Court Road, Cambridge, CB2 1QP, UK.

[2] Department of Biochemistry, University of Cambridge, Tennis Court Road, Cambridge, CB2 1QW, UK.

* Address correspondence to:

Department of Pathology, Cambridge University, Tennis Court Road, Cambridge, CB2 1QP, UK

Tel: (+44) 1223 333330

Email: cjm48@cam.ac.uk

## Abstract

*Plasmodium spp.* have different modes of cell division from most eukaryotes. Little is known about how these are controlled and cell-cycle checkpoints are particularly poorly characterised. However, parasites can arrest their cell cycle when treated with the frontline antimalarial drug artemisinin, and artemisinin-resistant parasites can modulate their cell-cycle progression, so it is very important to understand these aspects of *Plasmodium* biology. Here, we show that *P. falciparum* displays hallmarks of an intra-S-phase checkpoint when exposed to DNA damage, including acute reduction of DNA replication and phosphorylation of a putative damage-marker histone. Compounds that inhibit human checkpoint kinases can inhibit this arrest of DNA replication, and synergise with DNA damage in parasite killing. This suggests the existence of checkpoint kinase activity in *P. falciparum*, yet these kinases have no clear orthologues in *Plasmodium* genomes. We hypothesise that

phosphatidylinositol 3-kinase – an essential lipid kinase – may moonlight in this role: it is the closest homologue to a checkpoint kinase and is reportedly up-regulated in artemisinin-resistant parasites. Finally, we show that the cryptic checkpoint-kinase activity may also regulate the ring-stage survival phenotype after artemisinin damage, which resembles a G1/S checkpoint. Hence we suggest that checkpoint kinase inhibitors are candidates for synergy with artemisinin.

# Author summary

Malaria parasites cause illness by infecting human red blood cells, wherein they replicate to produce many new parasites within ~1-3 days. This is unusual because most cells (such as human cells) replicate simply by copying their genome and splitting in half – which is called binary fission – but malaria parasites make ~20 genome copies and then partition them simultaneously into 20 new cells – which is called schizogony. Here we studied how these parasites control schizogony. In particular, do they have 'checkpoints': the ability to pause the cell cycle for repair if the genome is damaged? We found that DNA damage during active replication did indeed cause hallmarks of a checkpoint. Key proteins that enforce this in other cells are surprisingly absent in malaria parasites, although DNA repair pathways and other regulatory pathways remain present. Furthermore, this checkpoint activity may be involved in the response to the antimalarial drug artemisinin: a response that parasites make by pausing their cycle before active replication begins. This could be important because it implies that inhibiting the checkpoint could exacerbate parasite killing by artemisinin-based drugs, similar to the way that some cancer therapies work by damaging DNA and also preventing the cancer cells from repairing it.

# Keywords

Malaria, *Plasmodium,* cell cycle, checkpoint, PI3K

# Introduction

46 *Plasmodium falciparum* is the most important cause of human malaria, giving rise to over half a
47 million deaths and hundreds of millions of clinical cases per year [1]. Besides being a major human
48 pathogen, it is also a highly unusual protozoan organism, distantly related to humans and other
49 model organisms, with distinctive features of cell and molecular biology. One of these is a non-
50 canonical cell cycle. Instead of dividing by binary fission, as in most model organisms, *Plasmodium*
51 parasites divide primarily by schizogony. After invading a host erythrocyte, they execute multiple,
52 asynchronous rounds of genome replication and nuclear division, generating a syncytium with
53 multiple nuclei within the same cytoplasm. This is followed by a relatively synchronous mass
54 cytokinesis event, partitioning as many as 20-30 nuclei and organelles into individual merozoites.

55 The complex events of schizogony are now being dissected in considerable molecular and
56 cellular detail [2-5] but fundamental questions remain about how the process is regulated.
57 Schizogony is not easily mapped onto the well-characterised cell cycle phases of G1, S, G2 and M.
58 After invading a new host cell, the parasite undergoes a pre-replicative growth phase broadly
59 analogous to G1. The haploid genome is then repeatedly replicated in a continuous S-phase without
60 once-and-only-once regulation, generating many new haploid nuclei. Different nuclei cease to
61 replicate at different times, and divide at different times, so there is no well-defined G2 and no
62 single M-phase [3].

63 *Plasmodium* replication is not controlled by conventional waves of cyclin and cyclin-
64 dependent kinase activity [6]. Nor is it apparently governed by conventional cell cycle checkpoints,
65 which usually operate at the G1/S transition, within S-phase, and at G2/M. Respectively, these
66 checkpoints delay the start of S-phase, arrest replication if DNA damage or replication stress is
67 detected, and prevent mitosis if a genome is incompletely replicated [7]. The *Plasmodium* genus,
68 however, encodes no clear homologues of the checkpoint kinases conserved in most eukaryotes
69 (animals, fungi and plants): Mec1 and Rad53 in *S. cerevisiae* and their homologues ATM/ATR and
70 Chk1/Chk2 in mammalian cells [6]. (By contrast, some parasites in the apicomplexan phylum,

71 including *Toxoplasma*, do retain homologues of the 'master regulators' Mec1/ATM/ATR, which are
72 phosphoinositide-3-kinase-like kinases (PIKKs), and checkpoints have been better characterised in
73 *Toxoplasma* [8-10]).

74 Nevertheless, eukaryotic cells generally do pause their cell cycles to ensure effective DNA
75 repair and faithful DNA replication – not only in metazoans, which must guard against cancer, but
76 also in protozoans. *Plasmodium* encodes most of the known DNA repair pathways [6, 11] and
77 generates relatively low rates of SNPs, indels and translocations during normal replication [12], so it
78 seems unlikely that it is entirely without checkpoints.

79 There is some evidence for a G1/S-like checkpoint: pre-replicative rings can undergo
80 'temporary growth arrest (TGA)' [13] in response to nutritional [14], temperature [15] or
81 antimalarial-drug [16, 17] stresses. TGA is particularly important under stress caused by the
82 antimalarial drug artemisinin, because it can contribute to treatment failure. However, there is no
83 molecular evidence as-yet that conventional checkpoint effectors are involved. A G1/S checkpoint
84 usually involves the cyclin/CDK complexes that drive S-phase entry, influenced positively by growth
85 factors or negatively by damage responsive kinases like PIKKs. TGA, by contrast, is defined only as a
86 'non-specific stress-response survival mechanism' [13]: induced by multiple stresses, possibly via
87 multiple molecular pathways.

88 An intra-S-phase checkpoint, meanwhile, should arrest S-phase specifically after DNA
89 damage or replication stress. After DNA damage, the transcriptional cascade that drives the
90 *Plasmodium* cell cycle can slow down, with DNA repair proteins and chromatin modifications being
91 upregulated [18], but the signals and transducers for this potential checkpoint are unknown.
92 (*Plasmodium* generally lacks validated markers for DNA damage and for direct responses to it.)
93 Indeed, the multi-nucleate, asynchronous nature of schizogony raises questions about how an intra-
94 S-phase checkpoint should or could be enforced. Replication itself is apparently regulated per-
95 nucleus, probably via individual accumulations of PCNA, together with non-canonical, chromatin-

96 bound CDK-related kinases like CRK4 [19]. Nevertheless, diffusible checkpoint kinases, potentially
97 affecting the whole cell, may not be incompatible with schizogony – at least in response to
98 exogenous DNA damage.

99 Finally, a G2/M checkpoint may be entirely absent because some *P. falciparum* mutants
100 perform grossly aberrant genome segregation but still undergo cytokinesis [20]. In fact, even in non-
101 mutants, certain phases of the lifecycle produce a high rate of zoids – particularly the rapid process
102 of gametogenesis inside the mosquito, when male cells produce and segregate eight new genomes
103 into mature, motile gametes in less than 15 minutes. In gametogenesis, cytokinesis proceeds even if
104 genome replication fails entirely [21, 22].

105 Here, we set out to investigate checkpoint responses to DNA damage in *Plasmodium,* using
106 newly developed molecular and cellular tools. We show that the hallmarks of an S-phase checkpoint
107 do occur in *P. falciparum*, despite the apparent absence of canonical PIKKs.

# 108 Results

## 109 Evidence for DNA-damage-responsive checkpoint activity in *P.* 110 *falciparum*

111 We used two complementary tools to investigate the response to DNA damage during S-phase in *P.*
112 *falciparum*, focussing at the levels of DNA and protein. Firstly, we labelled nascent DNA in
113 replicating parasites with a quantifiable modified nucleotide. This tested whether DNA replication
114 could be acutely arrested after damage: a hallmark of the intra-S-phase checkpoint [23, 24].
115 Secondly, we measured phosphorylation of histone H2A, which was recently identified as being
116 analogous to histone H2AX phosphorylation in mammalian cells [25]. Canonically, H2AX is
117 phosphorylated at chromatin sites of DNA damage [26, 27]. H2AX is absent in *Plasmodium*, but the

118 non-variant histone H2A can nevertheless be phosphorylated [25]. Importantly, this indicates an *in*
119 *trans*, kinase-driven, genuinely 'checkpoint-like' response.

120 To induce DNA damage, we used the well-characterised alkylating agent methyl methane
121 sulphonate (MMS), which alkylates DNA bases, particularly guanine and adenine [28]. In mammalian
122 cells, it induces an intra-S-phase checkpoint [23]. In *P. falciparum* parasites, it leads to DNA
123 breakage, as measured by comet assays [29] and concomitantly delays the cell cycle [18], but its
124 effect as a checkpoint inducer has not been explicitly addressed. In the *P. falciparum* 3D7 strain,
125 MMS had a 48h $IC_{50}$ of ~96µM (Fig S1A). Having established this, we performed highly acute assays
126 over just 1-2h, using 10x or 20x $IC_{50}$, to minimise non-specific or secondary effects. We confirmed
127 that parasites could substantially recover from this level of MMS exposure within one cell cycle,
128 although their maturation was delayed, as reported previously [18], and there was also a reduction
129 in merozoite numbers in mature schizonts (Fig S2).

130 DNA replication was acutely reduced in the 30 minutes following a 30-minute exposure to
131 MMS at 10x or 20x $IC_{50}$. Some reduction occurred throughout S-phase (~28-36 hours post invasion,
132 hpi) but it was most pronounced when DNA was damaged in early trophozoites (~32hpi) (Fig 1A).
133 Within a similar timeframe, histone H2A phosphorylation was moderately elevated (Fig 1B). We
134 recently reported that several DNA damaging agents, including MMS, could cause H2A
135 phosphorylation [30], but that the upregulation was transient and modest – usually less than 2-fold
136 over background levels – making it difficult to measure consistently. This was equally true when
137 MMS was used to induce H2A phosphorylation here (Fig 1B). (Previously published work measured
138 H2A phosphorylation in pre-replicative rings exposed to ionising radiation [25], whereas we
139 measured it in actively replicating trophozoites.) Therefore, we chose the replication-reduction
140 assay as a more robust readout for checkpoint activity in subsequent experiments.

141 ----------

142 **Fig 1:** Evidence for DNA-damage-responsive checkpoint activity in *P. falciparum*

143 A. BrdU incorporation into populations of trophozoites at three stages, after treatment with
144 MMS, as measured by ELISA. Parasites were treated with MMS for 1 h and BrdU was added
145 for the latter 30 mins. Means of two biological replicates, conducted in technical triplicate,
146 are shown; error bars show range. MMS treatments: 10x $IC_{50}$, 960 µM; 20x $IC_{50}$, 1.92 mM.
147 For each parasite stage, statistical testing was via ordinary one-way ANOVA and posthoc
148 Tukey's multiple comparisons test. *, P-value <0.05; comparisons not shown, ns. Pictures
149 show examples of trophozoites at each timepoint. Scale bar, 2µm.
150 B. Representative western blot of phosphorylated histone in trophozoite parasite lysate
151 treated with MMS (2 h, 10x $IC_{50}$). Phosphorylated histone signal was quantified versus
152 control histone H4: relative quantification is shown below the blot. Graph shows
153 quantifications from three biological replicate blots, relative to either H4 or Hsp70 as a
154 control protein. Unpaired two-tailed t-test: P-value = 0.0354.
155 ----------

## 156 Possible mediators of checkpoint activity in *P. falciparum*

157 When the intra-S-phase checkpoint is triggered in other eukaryotes, both histone phosphorylation
158 and arrest of DNA replication are transduced through PIKKs [24, 26]. Since Figure 1 shows that these
159 phenotypes also appear in *P. falciparum,* a transducing kinase activity should be present. However,
160 orthologues of ATM/ATR are not obvious by similarity searches in the *P. falciparum* genome [6]. To
161 test for the presence or loss of such orthologues more thoroughly, we performed an extensive
162 phylogenetic analysis of PIKK homologues throughout apicomplexans and other major eukaryotic
163 lineages (Fig 2). In this analysis, PI3K and PI4K kinases formed an outgroup relative to all ATM/ATR-
164 like proteins. ATR homologues were found in most apicomplexans, and some – like *T. gondii* –
165 clearly retained homologues of both ATM and ATR. Other apicomplexans, including
166 *Cryptosporidium*, *Babesia* and *Theileria*, had apparently independently lost the ATM homologue,
167 indicating a propensity for loss of PIKKs in Apicomplexa. *Plasmodium* spp. were unique in having lost

168 both ATM and ATR, retaining no apparent PIKKs at all. The closest PIKK homologues in any
169 *Plasmodium* genome were the lipid kinases PI3K and PI4K (Fig 2, Fig S3), which are also present
170 throughout most apicomplexans [31]. (*Theileria* was seemingly unique in having lost its PI3K
171 homologue, possibly due to a lifecycle conducted free in the cytoplasm of leukocytes, which may
172 supply this activity.) Notably, the closest *Plasmodium* homologue, PI3K, has been reported to be
173 overexpressed in artemisinin resistant parasites [32], which can alter their cell cycle dynamics.
174 Accordingly, we hypothesised that PI3K might act as a checkpoint kinase in *Plasmodium.*
175 ----------

176 **Fig 2:** *Plasmodium* encodes no homologues of PIKK checkpoint kinases
177 A phylogeny inferred for amino acid protein sequences of ATR, ATM, and TOR homologues sampled
178 from broad eukaryote groups. Apicomplexa homologues of PI3K and PI4K (the most closely related
179 proteins to ATR and ATM present in *Plasmodium*) and characterised homologues of PI3K and PI4K
180 from *Saccharomyces cerevisiae* and *Homo sapiens* were included as an outgroup. Support values,
181 displayed as percentages, were generated from 1000 ultrafast bootstrap replicates [33] and only
182 support values ≥ 90, indicating strongly supported clades, are shown. The scale bar represents the
183 number of amino acid substitutions per site. A fully-expanded version of this tree with no collapsed
184 clades and displaying sequence accessions is provided in the source data.
185

186 *Pf*PI3K is the only phosphoinositide 3-kinase of the six phosphoinositide kinases in
187 *Plasmodium* [31]: it is a well-validated, essential lipid kinase [34] with roles in nutrient uptake and
188 vesicle trafficking [35, 36]. We hypothesised that it might also 'moonlight' as a protein kinase, which
189 would not be unprecedented, as other PI3Ks can to act on proteins as well as lipids. For example,
190 humans encode a large family of PI3Ks, and the type-1 PI3Ks can phosphorylate protein substrates
191 such as cytokine receptors, as well as auto-phosphorylating themselves [37, 38]. The sole
192 *Plasmodium* enzyme is a type-3 PI3K, and thus far these are proven only to phosphorylate lipids [34].

193 If our hypothesis was correct, then *Pf*PI3K should have some activity within the nucleus,
194 phosphorylating substrates such as histone H2A. To track the protein *in cellulo,* we raised peptide
195 antibodies (modelling for peptide selection is shown in Fig S4A), which detected a protein of the
196 correct 256kDa size (Fig 3A). In immunofluorescence, *Pf*PI3K appeared dispersed and cytoplasmic
197 (Fig 3B, Fig S4B), consistent with a previous publication that suggested a location in transport
198 vesicles [36]. We did not detect any substantial re-location to the nucleus upon DNA damage (Fig
199 3C). However, we recently showed that the ATM and ATR homologues in *Toxoplasma* are likewise
200 dispersed throughout the cell and do not detectably relocate to the nucleus after DNA damage, but
201 they are nevertheless able to mediate checkpoint phenotypes such as histone phosphorylation [39].

202 ----------

203 **Fig 3:** *Pf*PI3K does not visibly relocate to the nucleus upon DNA damage

204 A. Western blots showing detection of *Pf*PI3K by two antisera raised to *Pf*PI3K peptides.
205 Replicate lanes from the same blot of protein lysate from late-stage *P. falciparum* were
206 exposed to either pre-immune or immune serum. Histone H4 was used as a loading control.
207 B. Immunofluorescence assay (IFA) showing location of *Pf*PI3K (detected by antiserum 1) in *P.*
208 *falciparum*. 2-3 representative cells are shown per stage. Scale bar 1 μm.
209 C. IFA showing *Pf*PI3K in *P. falciparum* after DNA damage: 1 h treatment with 5x or 10x $IC_{50}$ of
210 DHA or MMS on late-stage parasites. One representative cell per condition is shown. Scale
211 bar 1μm.

212 ----------

213 Further molecular-genetic experiments were precluded because the *Pf*PI3K enzyme is
214 essential (probably due to its unique lipid kinase activity). Several attempts were made to 3' tag the
215 gene for a partial, non-lethal conditional knockdown instead, but these failed, probably because the
216 enzyme's active site is encoded at the extreme 3' end and may become mis-folded after 3' tagging.
217 Similar attempts by other groups to manipulate this gene were either unsuccessful or gave no

218 phenotype [40, 41]. The large size of the *PfPI3K* gene (6.6kb) precluded overexpression, dominant-
219 negative overexpression or recombinant protein production for enzyme-activity assays. Attempts
220 were also made to immunoprecipitate the native protein with its potential substrates, but only a
221 single *Pf*PI3K peptide was detected across several immunoprecipitation attempts – probably because
222 the kinase is lowly expressed, very large and unstable *in vitro*, or lacking suitable tryptic digest sites
223 (notably, it was likewise undetected, despite its large size, in two dedicated proteomic studies that
224 examined the nuclear versus cytoplasmic proteomes in *P. falciparum* [42, 43]). Thus, the putative
225 PIKK-like activity of *Pf*PI3K remained neither evidenced nor disproved. Future work using state-of-
226 the-art proteomic methods like hyperLOPIT for protein localisation (recently achieved in *T. gondii*
227 [44]) or proximity-labelling of protein partners via BioID [45] could shed light on a putative intra-
228 nuclear role for *Pf*PI3K.

## 229 The mediator of DNA-damage checkpoint responses in *Plasmodium* 230 is sensitive to PIKK inhibitors

231 Despite the lack of conclusive evidence for *Pf*PI3K as a checkpoint kinase, a divergent PIKK-like
232 kinase may nevertheless exist in *P. falciparum*, and hence we attempted to inhibit it with PIKK
233 inhibitors. We chose two compounds that had validated specificity for human ATM and ATR
234 respectively (but not for human PI3Ks), KU-55933 and VE-821 [46, 47]. If an ATM-like and/or ATR-
235 like activity existed in *P. falciparum*, either in *Pf*PI3K or in another protein, these compounds might
236 specifically inhibit it. We first determined their 48h $IC_{50}$ values on *P. falciparum* (3D7 strain): KU-
237 55933 had an $IC_{50}$ in the micromolar range and VE-821, in the nanomolar range (Fig 4A, Fig S1B).

238 ----------

239 **Fig 4:** Inhibitors of human PIKKs synergise with the DNA-damaging agent MMS in *P. falciparum*

240 A. Inhibition of parasite growth by VE-821 and KU-55933 (molecular structures of each
241 inhibitor are shown). Growth curves from five independent malaria SYBR green I-based

242 fluorescence (MSF) assays: percentage parasite growth is plotted as a function of drug
243 concentration, error bars are standard errors of the means. Mean $IC_{50}$s from all experiments
244 are shown (individual $IC_{50}$ values from replicate experiments are in Fig S1B).
245 B. Isobolograms plotted as fractional inhibitory concentrations (FIC) of combinations of MMS
246 and VE-821 or KU-55933, as determined by MSF assay. FIC calculations were completed for
247 each combination by dividing the measured "apparent" $IC_{50}$ values for individual drugs in the
248 different combinations by $IC_{50}$ values obtained when the drugs were used alone. Each curve
249 represents a different biological replicate experiment. The mean FIC ($\Sigma FIC(FIC_A+FIC_B)$) is
250 shown, with range. The type of relationship was defined as moderately synergistic based on
251 well-established criteria: ∑FIC <0.5, substantial synergism; ∑FIC <1, moderate synergism;
252 ∑FIC ≥1 and <2, additive interaction; ∑FIC ≥2 and <4, slight antagonism and ∑FIC >4, marked
253 antagonism [48].
254 C. BrdU incorporation into 30-32 hpi trophozoites after treatment with MMS, VE-821, KU-
255 55933, geneticin and combinations of these, measured by ELISA. Parasites were treated with
256 10x $IC_{50}$ of drug for 1 h and BrdU was added for the latter 30 mins. Six biological replicates
257 are plotted, each completed in technical triplicate. Mean and standard deviation error bars
258 are plotted, values normalised to control (set to 100%) in each replicate. Concentrations of
259 drugs used: MMS 960 $\mu$M, VE-821 1.62 $\mu$M, KU-55933 400 $\mu$M, geneticin 1500 $\mu$g/ml.
260 Ordinary one-way ANOVA and posthoc Tukey's multiple comparisons test of control vs all
261 and MMS vs all was completed; P-values: *, <0.05; **, <0.01; ***, <0.001; ****, <0.0001;
262 comparisons not shown, ns.
263 ----------

264 Both inhibitors clearly synergised with MMS in a 48h isobologram analysis, particularly
265 strongly in the case of VE-821, suggesting activity within the same pathway (Fig 4B). Control
266 compounds that kill parasites but are not known to cause DNA damage – the antibiotics blasticidin
267 and geneticin – did not synergise with MMS (Fig S5). Furthermore, when parasites were exposed to

268 high-dose MMS (10x $IC_{50}$, as in Figure 1) simultaneously with KU-55933 or VE-821, the inhibitors
269 ablated the acute reduction in DNA replication caused by MMS, whereas co-exposure to the control
270 antibiotic geneticin did not (Fig 4C). In this short 1h assay, we used the PIKK inhibitors at only their
271 48h $IC_{50}$ levels, to minimise any negative effects from the inhibitors alone. Indeed, within the
272 timeframe of the assay the inhibitors alone did not significantly affect DNA replication (Fig 4C).
273 Overall, these data strongly supported the existence of a cryptic PIKK activity, responsible for a
274 genuine intra-S-phase checkpoint via *in trans* kinase activity.

275 Having established this, we sought to link the inhibitors to their putative target of *Pf*PI3K, on
276 the basis that parasites with more or less *Pf*PI3K would be expected to have, respectively, lower or
277 higher inhibitor sensitivity. Although no successful inducible knockdown of *Pf*PI3K has yet been
278 created (as noted above), the first inducible knockout was very recently published [49]. We
279 obtained this and tested knockout parasites for any change in sensitivity to PIKK inhibitors.
280 Unfortunately, knockout parasites did not prove amenable to standard 48h (or 72h) drug-sensitivity
281 assays (Fig S6). This was because they displayed a delayed-death phenotype, well described in [49],
282 that rendered them relatively healthy through cycle-2 after induction of the knockout, but dead
283 before cycle-3. Accordingly, they were not differently sensitive to VE-821 or KU-55933 in MSF assays
284 conducted over 48h in cycles 1-2, but all parasites died before a longer 72h MSF assay could be read.

285 The converse approach of overexpressing PI3K for a reduction in inhibitor sensitivity was also
286 attempted. Due to the prohibitively large size of *Pf*PI3K, we used a PbAC artificial chromosome to
287 express an extra copy of the *P. berghei* PI3K homologue in *P. knowlesi*: a system recently
288 published as a novel chemogenomic screening platform [50]. Unfortunately, *Pb*PI3K transgene
289 overexpression proved in this instance to be weak and resultant changes in drug sensitivity were
290 marginal and not statistically-significant (similar to the results shown in figure S6).

291 **The antimalarial drug dihydroartemisinin induces DNA replication**

292 **arrest in *P. falciparum***

293 MMS is a useful, well-characterised DNA-damaging agent, but it is not an antimalarial drug. We
294 were particularly interested in the potential DNA-damaging activity of antimalarial drugs, because if
295 parasites do make checkpoint responses to such drugs, then their antimalarial activity might be
296 potentiated by inhibiting checkpoint kinases. Artemisinin is such a drug: it has non-specific alkylating
297 activity that may affect both proteins and DNA [51, 52]. There are similarities between the
298 parasite's response to dihydroartemisinin (DHA, the active metabolite of artemisinin) and MMS in
299 terms of DNA breakage [51, 53], delay in the parasite's transcriptional cascade, and upregulation of
300 DNA repair genes [18]. Indeed, we found that DHA induced H2A phosphorylation, at all stages of the
301 cycle but particularly in pre-replicative ring stages (~3-fold upregulation after 4h exposure to $IC_{50}$
302 DHA, (Fig 5A)). This confirmed that DHA does indeed cause damage that activates a putative histone
303 kinase, and furthermore that it can cause this damage prior to S-phase.

304 Using the replication-reduction assay, we saw that in replicating parasites, DHA caused an
305 acute reduction in nascent DNA replication, similar to MMS (Fig 5B). However, unlike MMS, this was
306 not ablated by the PIKK inhibitors KU-55933 and VE-821. Consistent with this difference, the
307 inhibitors did not synergise with DHA in isobologram analysis (Fig 5C). This suggested that although
308 both DHA and MMS may damage DNA, they differ in either the type of damage or the cellular
309 response thereto in terms of inducing an intra-S-phase checkpoint.

310 ----------

311 **Fig 5:** The antimalarial drug dihydroartemisinin induces a DNA replication arrest in *P. falciparum*

312 A. Western blot of phosphorylated histones in ring, trophozoite and schizont-stage parasites
313 treated with DHA (4h, $IC_{50}$ (3nM)). Phosphorylated histone signal was quantified versus
314 control histone H4: relative quantification is shown below the blot.

315 B. BrdU incorporation into 30-32 hpi trophozoites after treatment with DHA, VE-821, KU-55933
316 and combination treatments. Parasites were treated with 10X $IC_{50}$ of drug for 1 h and BrdU
317 was added for the latter 30 mins. Five biological replicates were plotted, each completed in
318 technical triplicate. Mean and standard deviation error bars are plotted; values were
319 normalised to control (set to 100%) in each replicate. Concentrations of drugs used: DHA 45
320 nM, VE-821 1.62 $\mu$M, KU-55933 400 $\mu$M. Statistical testing by ordinary one-way ANOVA and
321 posthoc Tukey's multiple comparisons test of control vs all and DHA vs all; P-values: *, <0.05;
322 comparisons not shown, ns.
323 C. Isobolograms plotted as Figure 4B. Each curve is a biological replicate and the mean FIC
324 ($\Sigma FIC(FIC_A+FIC_B)$) is shown, with range. The relationship between DHA and either VE-821 or
325 KU55933 was defined as additive.

326 ----------

## 327 Ring-stage survival after artemisinin damage is affected by PIKK
## 328 inhibitors

329 Cell-cycle checkpoint activity in *P. falciparum* may not be limited to an intra-S-phase checkpoint:
330 most eukaryotic cells also operate a G1/S checkpoint, delaying S-phase entry if cells are damaged,
331 starved or stressed. This may be analogous to the 'TGA' arrest or 'dormancy' that occurs in ring-
332 stage parasites after various stressors, including artemisinin treatment [13]. We therefore set out to
333 establish whether ring-stage dormancy induced by DHA actually represents a classical, PIKK-
334 mediated G1/S checkpoint, responsive to the DNA damage that can be exerted upon ring stages by
335 DHA (as shown in figure 5A).

336 We conducted the ring-stage survival assay (RSA) on parasites treated with DHA in the
337 presence or absence of PIKK inhibitors. In this assay, pre-replicative early-ring-stage parasites are
338 damaged with a pulse of DHA: most of them die, but some successfully arrest and thence survive.

339 The more parasites are able to do this, the higher the subsequent recovery of viable parasites. We
340 reasoned that if successful arrest is due to PIKK-mediated checkpoint activity, then PIKK inhibitors
341 should reduce ring-stage survival. These experiments were conducted in the 3D7 strain and also in
342 the Cambodian strain MRA-1252. MRA-1252 was derived from a naturally-arising DHA-resistant
343 strain, which was genetically reverted back to a sensitive phenotype by reverting the resistance
344 mutation in the gene encoding Kelch13 [54]. Its genetic background is otherwise that of a S.E. Asian
345 DHA-resistant line. Both 3D7 and MRA-1252 are highly sensitive to artemisinin, so we used the
346 'extended recovery ring-stage survival assay' (eRRSA), which detects recovered parasites very
347 sensitively after 72h via quantitative PCR [55].

348 Figure 6A shows that PIKK inhibitors, particularly KU-55933, did indeed exacerbate the killing
349 of ring-stage parasites by DHA. Differences were only subtle and parallel assays using the more
350 common but less sensitive flow cytometric assessment of live/dead cells to read the RSA likewise
351 showed only marginal differences (Fig S7). However, in both 3D7 and MRA-1252, triplicate eRRSAs
352 showed that survival trended downwards when DHA was combined with either inhibitor. Neither
353 condition (DHA + VE-821 or DHA + KU-55933) reached statistical significance versus survival after
354 DHA alone, but the p-values versus control were < 0.0001 rather than 0.001. As above, we
355 minimised any negative effects of the inhibitors themselves by using them at a low level – only half
356 of the 48h $IC_{50}$. We confirmed that this exposure alone for 6h did not affect parasite survival after
357 72h (Fig 6B).

358 ----------

359 **Fig 6**: Ring-stage survival is affected by PIKK inhibitors

360 Data in A-D are from eRRSA assays on the strains 3D7, MRA-1252 and MRA-1240. Samples were
361 treated with DMSO (the control condition), VE-821, KU-55933, DHA and combinations of these. Drug
362 concentrations: VE-821, 81 nM (0.5X $IC_{50}$); KU-55933, 20 μM (0.5X $IC_{50}$); DMSO, 0.02%; DHA, 700 nM.
363 Values plotted are the means of -log(foldchange = 2^(DHA-DMSO)) for each treatment. Midline

364 represents the mean and boxes show min to max from three biological replicates, each conducted in
365 technical triplicate. Statistical testing by ordinary one-way ANOVA and Dunnett's multiple
366 comparisons test, comparing all means to the mean value from DMSO- or DHA-treated samples. P-
367 values: *, <0.05; **, <0.01; ***, <0.001; ****, <0.0001. Differences between DHA-treated samples
368 and treatments other than the control did not reach statistical significance.

369 A. Ring-stage DHA-sensitive parasite strains, 3D7 or MRA-1252, were treated with DMSO (control
370 condition), DHA and inhibitors VE-821 or KU-55933 in combination with DHA for a 6 h pulse, then
371 left to recover for 72 h.

372 B. Control experiments without DHA: ring-stage 3D7 or MRA-1252 parasites were treated with
373 DMSO or inhibitors VE-821 or KU-55933 for a 6 h pulse, then left to recover for 72 h.

374 C. Ring-stages of the DHA-resistant parasite strain MRA-1240 were treated with DMSO (control
375 condition), DHA and inhibitors VE-821 or KU-55933 in combination with DHA for a 6 h pulse, then
376 left to recover for 72 h.

377 D. Control experiment without DHA: ring-stage MRA-1240 parasites were treated with DMSO or
378 inhibitors VE-821 or KU-55933 for a 6 h pulse, then left to recover for 72 h.

379 E. Inhibition of growth over a full 48h growth cycle by MMS, VE-821 and KU55933 was measured in
380 the strains 3D7, MRA-1252 and MRA-1240 via MSF assay. $IC_{50}$s were calculated from at least
381 three independent experiments and all values are plotted, with the midline showing the mean
382 and error bars showing standard deviation. MSF growth curves are in Fig S1C.

383 ----------

384 These RSAs did not show conclusively that 'TGA' after artemisinin damage represents a true
385 G1/S checkpoint. However, they did suggest that such a checkpoint, mediated by a cryptic PIKK, may
386 contribute to ring-stage survival. Hence, the cryptic PIKK must be active throughout the cell cycle,
387 not only in actively replicating trophozoites.

388 When the same assay was conducted on DHA-resistant parasites (the parent strain of MRA-
389 1252, called MRA-1240) the result differed. As expected, DHA survival was much better in MRA-
390 1240, and PIKK inhibitors had no negative effect on this survival (Fig 6C). If anything, there was a
391 trend towards better growth and better DHA survival when MRA-1240 was exposed to PIKK
392 inhibitors (Fig 6D). Hence, when a Kelch13 mutation was present, conferring DHA resistance, any
393 contribution of checkpoint activity to parasite survival was apparently ablated.

## 394 Artemisinin-resistant parasites are cross-resistant to MMS and VE-
## 395 821, but not to KU-55933

396 We hypothesised that artemisinin-resistant (Kelch13 mutant) parasites might not require 'G1/S'
397 checkpoint activity to survive DHA damage because they are more efficient at DNA repair. Several
398 mutations in DNA repair genes have been identified in resistant strains [52], although the pathway(s)
399 leading to improved DNA repair remain to be fully characterised. We checked whether the DHA-
400 resistant line MRA-1240 was cross-resistant to MMS, and its $IC_{50}$ was indeed significantly higher than
401 that of the matched sensitive line MRA-1252 (and also higher than that of 3D7) (Fig 6E, left panel; Fig
402 S1C). Since the point mutation in Kelch13 is the only difference between the two Cambodian MRA
403 lines, a genetic background of enhanced DNA repair cannot fully account for this.

404 One other explanation for an improved DNA repair capacity in resistant parasites could be
405 that they have hyper-active checkpoint activity (possibly due to Kelch13-associated over-expression
406 of PI3K [32]) and that this stimulates hyperactive DNA repair. This explanation *would* be consistent
407 with MRA-1240 (Kelch13-mutant) and MRA-1252 (revertant) having different sensitivities to MMS.
408 If so, the Kelch13 mutant state would also be expected to correlate with reduced sensitivity to PIKK
409 inhibitors. Indeed, MRA-1240 was much less sensitive to the VE-821 inhibitor (Fig 6E, middle panel;
410 Fig S1C) – so much so that it was difficult to measure a consistent $IC_{50}$ via MSF assay. Curiously,
411 however, the same line was not less sensitive to KU-55933 (Fig 6E, right panel; Fig S1C). This was the

412 first instance in which VE-821 and KU-55933 had shown a clear difference in their effects on *P.*
413 *falciparum.* It may suggest that more than one checkpoint protein is required, at least in the MRA-
414 1240/1252 genetic background, and that one of the inhibitors has a broader inhibitory spectrum
415 than the other. For example, *Pf*PI3K may indeed moonlight as a checkpoint kinase, uniquely
416 unregulated after Kelch13 mutation and uniquely inhibited by VE-821, whereas *Pf*PI4K and/or other
417 'off-target' kinases may also act in certain checkpoint pathways, and KU-55933 may inhibit this
418 broader kinase spectrum, which is unaffected by the Kelch13 mutation in MRA-1240.

419 These speculations urgently require the conditional genetic manipulation of at least two
420 large, essential kinase-encoding genes, *PfPI3K* and *PfPI4K* – in parallel, in a molecular-genetic system
421 that can achieve meaningful levels of knockdown without cell death.

# 422 Discussion

423 This work provides the first evidence that *Plasmodium* parasites during blood-stage schizogony can
424 enforce an intra-S-phase checkpoint. The checkpoint is evidenced by an acute reduction in the rate
425 of DNA replication and increased phosphorylation of histone H2A in a position analogous to the
426 canonical DNA damage marker H2AX. *P. falciparum* was previously shown to slow its cell-cycle
427 progression after DNA damage [18] but it was not clear if this occurred through cell-cycle checkpoint
428 activity (partly because the *Plasmodium* system lacked validated DNA damage markers, signals or
429 transducers thereof). Markers still remain limited – there are, for example, no cyclin markers for
430 cell-cycle phases, and the H2A phosphorylation that has been reported as a DNA damage marker in
431 ring stages [25] is not, in our hands, a very strong marker in trophozoite stages (possibly because
432 background levels are higher in actively-replicating parasites). However, the ability to measure
433 nascent DNA replication in *Plasmodium* [56] does now allow intra-S-phase checkpoint activity to be
434 measured. Thus we showed that DNA replication was acutely arrested by two distinct alkylating
435 agents, MMS and the antimalarial drug DHA.

436 The transducer(s) of checkpoint activity in *Plasmodium* remain cryptic. *Plasmodium* spp.
437 lack identifiable orthologues of PIKK kinases, in contrast to many apicomplexans including *T. gondii*
438 [39]. Nevertheless, such activity is apparently present, because the reduction in replication caused
439 by MMS was ablated by well-validated inhibitors of human PIKKs. Hence it must be induced *in trans*
440 by a genuine kinase-mediated signalling cascade (also consistent with H2A phosphorylation), rather
441 than occurring simply because alkylated bases physically block the movement of replisomes.
442 Interestingly, DHA differed from MMS in this respect: it also affected DNA replication, but PIKK
443 inhibitors did not ameliorate this. Possibly the acute effect of DHA – which is a larger molecule than
444 MMS – *is* primarily to block replisomes via bulky DNA adducts (a documented effect of alkylating
445 agents in human cells [23]), and these cannot be bypassed whether a checkpoint kinase is active or
446 not, while a lesser role is played by *in trans* checkpoint signalling after DHA damage.

447 Other, more complex, explanations for the difference in response to MMS versus DHA are
448 also possible. For example, slow DNA replication can, in general, stimulate compensatory activation
449 of extra replication origins [57], but when DNA damage is sensed, checkpoint kinases act *in trans* to
450 suppress such origin firing [23]. If checkpoint kinases are inhibited, then extra origins may fire
451 regardless, hence MMS-damaged cells may keep replicating and encountering more damage, so
452 genome replication ultimately fails to complete. This would explain how MMS and PIKK inhibitors
453 ultimately synergise in cell killing. Perhaps the broader-spectrum damage that DHA causes to
454 proteins as well as DNA [51], and/or the oxidative stress that it generates [53] means that
455 compensatory origin firing does not happen, whether a checkpoint is activated or not. Hence PIKK
456 inhibitors would not synergise with DHA in cell killing. To evidence these rather complex
457 hypotheses, precision measurement of DNA replication dynamics at single-molecule resolution after
458 different types of damage will be needed. This has been achieved in human cells [23], and is now in
459 development for *Plasmodium*.

460 Turning to the possibility of a pre-replicative G1/S checkpoint, the evidence for this being
461 mediated by a PIKK-like kinase is not conclusive, but nevertheless tantalising. In the RSA, which
462 measures DHA killing of pre-replicative rings, PIKK inhibitors exacerbated parasite killing. The effect
463 was modest, so if a classical (kinase-enforced) G1/S checkpoint does exist, it is probably not the sole
464 defining factor in survival of artemininin-induced dormancy. Nevertheless, the trend was consistent
465 (albeit not statistically significant) in triplicate assays across two genetically-distinct DHA-sensitive
466 strains, 3D7 and MRA-1252. Checkpoint kinase activity could help to protect ring-stage cells,
467 perhaps by detecting DNA damage, stimulating repair, and preventing S-phase entry until repair is
468 complete. By contrast, a DHA-resistant strain showed no effect of PIKK inhibitors. This may be
469 because it can already suppress DHA activation in early rings and thus protect itself from DNA
470 damage; or alternatively, it may still sustain some damage, but be rescued by hyperactive DNA
471 repair [52]. Consistent with this latter hypothesis, it was recently shown that when *Pf*PI3K is
472 inducibly knocked out in a DHA-resistant Kelch-13 mutant background, these parasites become less
473 DHA resistant – perhaps because they can no longer resist or repair DHA-related DNA damage when
474 the mediating kinase, PI3K, is lost [49].

475 If there is indeed hyperactive DNA repair in the MRA-1240 line, it cannot be conferred by a
476 DHA-resistant genetic background because the matched strain MRA-1252 was not cross-resistant to
477 MMS, whereas MRA-1240 was. However, it could be because the Kelch13 mutation, uniquely
478 present in MRA-1240, confers hyper-checkpoint activity, thus stimulating hyperactive DNA repair. In
479 any case, these data raise the intriguing possibility that artemisinin drugs could synergise with
480 checkpoint inhibitors in killing ring-stage parasites; the caveat being that this might only work well in
481 sensitive, not resistant, strains.

482 It is an attractive idea that *Pf*PI3K is the cryptic checkpoint kinase, particularly if Kelch13
483 mutant strains contain more *Pf*PI3K [32]. However, we were not yet able to prove or disprove this,
484 owing to the difficulty of manipulating the large, essential *PfPI3K* gene. Broad-spectrum inhibitors

485 such as wortmannin were used in previous work [36], but these are slow-killing and unable to
486 separate lipid-kinase from putative protein-kinase activity. We used PIKK inhibitors instead, hoping
487 to isolate a putative protein kinase activity. The fact that our PIKK inhibitors did not synergise with
488 DHA in MSF assays, whereas specific inhibitors of distinct human PI3Ks (i.e. lipid kinases) *have* been
489 reported to do so [58], may suggest that this succeeded, and that VE-821 and KU-55933 do target a
490 distinct activity in *Plasmodium*. They may, of course, merely affect irrelevant off-targets – multiple
491 or unexpected kinases, or perhaps even non-kinases. As an example, a repurposed human-kinase
492 inhibitor was recently deployed to target *Plasmodium* PK6, but it actually targeted haem
493 detoxification pathways as well [59]. More likely, however, is that these inhibitors genuinely inhibit
494 a *Plasmodium* checkpoint kinase – which may reside in *Pf*PI3K, *Pf*PI4K, or another radically divergent
495 protein. *Plasmodium* contains many kinases whose roles are yet-unknown [60], and the *Plasmodium*
496 cell cycle is driven by markedly divergent kinases such as CRK4 [61], so it is entirely possible that
497 *Plasmodium* checkpoints have evolved to be enforced by novel kinase(s) as well. In conclusion, we
498 present new evidence for measurable cell-cycle checkpoint activity in *Plasmodium*. We also raise
499 the considerable challenge of unambiguously identifying its mediators in this divergent eukaryotic
500 parasite.

# 501 Methods

## 502 Parasite cultures

503 *Plasmodium falciparum* cultures were grown in 2% or 4% haematocrit human erythrocytes
504 (Research Red Cells obtained from the NHS Blood & Transplant service), in RPMI 1640 (Sigma,
505 R4130) supplemented with 2.3 g/L sodium bicarbonate, 50 mg/L hypoxanthine (Sigma, H9377), 25
506 µg/L gentamicin (Melford Laboratories, G38000-1), 2.5 g/L Albumax II and 5% human serum.
507 Parasites were cultured under a 1% $O_2$/ 3% $CO_2$/ 96% $N_2$ gaseous atmosphere at 37 °C.

508 ## Parasite strains

509 Parasite strains used were: 3D7, 3D7 pTK, iPI3K-ko (also in the 3D7 background) [49], MRA-1240 and
510 MRA-1252. 3D7 pTK carries a thymidine kinase transgene to allow incorporation of
511 bromodeoxyuridine (BrdU) for monitoring DNA replication [56]. The iPI3K-ko line carries a D-Cre-
512 inducible deletion module for the C-terminal part of the *PI3K* gene [49]. MRA-1240 and MRA-1252
513 are matched artemisinin-resistant and sensitive Cambodian field lines, respectively [54], obtained
514 through BEI Resources (NIAID, NIH). Parasites were synchronised as in [62]. The PI3K inducible
515 knockout was enforced by treating ring-stage parasites with 100nM rapamycin (or DMSO vehicle for
516 the control), as described by the original authors [49], before conducting MSF assays 24-72h or 24-
517 96h later.

518

519 ## Database sampling and phylogenetic analysis

520 The phylogeny (Fig 2) for ATM, ATR, TOR, PI3K and PI4K homologues was inferred by following a
521 computational workflow (https://github.com/camwallerlab/Methods-for-phylogenetic-analysis-of-
522 plastid-translocons) developed as part of a previous study [63]. In summary, this workflow involved
523 sampling a custom protein sequence database that included data for major eukaryotic groups from
524 UniProt [64] and the Marine Microbial Eukaryote Transcriptome Sequencing Project [65], as well as
525 data for apicomplexans and close relatives from VEuPathDB [66] and two previous studies [67, 68].
526 This custom database was then sampled for ATM, ATR and TOR homologues using the program
527 blastp (BLAST+ version 2.11.0 [69]), for which characterised homologues of these proteins from
528 selected model organisms were used as search queries. The dataset of possible ATM, ATR and TOR
529 homologues obtained was then clustered with CD-HIT [70] to remove highly similar sequences,
530 thereby reducing overall redundancy of the dataset. PI3K and PI4K homologues from *Plasmodium*
531 and other apicomplexans, as well as characterised homologues from *Saccharomyces cerevisiae* and
532 *Homo sapiens* were incorporated into the dataset as a phylogenetic outgroup for the ATM, ATR and

533 TOR proteins. Iterative rounds of alignment were then performed using mafft (MAFFT version 7.475
534 [71]), conserved site selection using trimal with "gappyout" mode (trimAl version 1.4 [72]), and tree
535 inference with FastTreeMP (FastTree version 2.1.11 [73]) using the default settings. For each
536 iterlation, sequences that aligned poorly or were so dissimilar from the rest of the sequences in the
537 dataset that they were unlikely to be ATM, ATR or TOR homologues, but rather false positives of the
538 described sampling strategy, were manually identified and removed from the dataset. The final
539 curated dataset that these iterations obtained was then aligned using mafft-linsi (MAFFT version
540 7.475 [71]) and conserved sites were selected using trimal with "gappyout" mode (trimAl version 1.4
541 [72]). A phylogeny was then inferred from this dataset using the program iqtree2 (IQ-TREE version
542 2.1.2 [74]) with 1000 ultrafast bootstrap replicates (UFBoot2 [33]) and using the best-fitting model,
543 LG+F+I+G4 ([75]) that was chosen according to the Bayesian Information Criterion by ModelFinder
544 [76], all implemented within iqtree2. The protein sequences, alignment, and tree inference output
545 files used to generate the phylogeny are provided as source data.

546

547 ## BrdU Enzyme-linked immunosorbent assay (ELISA)

548 ELISA was carried out as per [56]. In brief, tightly synchronised *P. falciparum* 3D7 pTK parasites were
549 collected at 4% parasitaemia and 4% haematocrit at 28 hpi, 32 hpi and 36 hpi. They were labelled
550 with BrdU (100 µM, Sigma) for 30 min and then collected for ELISA, or treated with MMS at 10 x $IC_{50}$
551 (960 µM) or 20 x $IC_{50}$ (1,920 µM) for 30 min prior to BrdU labelling. In further experiments, parasites
552 at 30-32 hpi were exposed to either MMS alone (10x $IC_{50}$), MMS+VE-821 (1x $IC_{50}$), MMS+KU-55933
553 (1x $IC_{50}$), VE-821 alone, KU-55933 alone, DHA alone (10x $IC_{50}$), DHA+VE-821, DHA+KU-55933 or no
554 drugs, then processed as above.

555 **Immunofluorescence**

556 Air-dried thick blood smears were fixed with 4% paraformaldehyde in PBS for 10 min and
557 permeabilised for 10 min with 0.05% triton in PBS. Slides were then blocked for 1 h in 1% BSA/PBS.

558 The primary antibody was added in blocking buffer for 1 h under a coverslip. After 3x 5 min washes
559 in PBS, the secondary antibody was added to slides for 1 h. The slides were washed with PBS for 5
560 min, 120 µl of 2 µg/ml DAPI solution was added for 10 min and then the slides washed again with
561 PBS for 5 min. Coverslips were mounted on slides in Prolong® Diamond (Invitrogen) and allowed to
562 dry overnight at 4 °C. Images were acquired using a Nikon Eclipse Ti widefield microscope with a
563 Nikon objective lens (Plan APO, 100x/1.45 oil), and a Hamamatsu C11440, ORCA Flash 4.0 camera.
564 Images were processed using the NIS-Elements software and ImageJ (v.1.51w).

## 565 Malaria SYBR Green-1 Fluorescence (MSF) assay

566 MSF assays were conducted as in [77]. 100 µM chloroquine (Merck) was used as a control for
567 parasite death. Data were analysed and graphs plotted in GraphPad Prism.

## 568 Isobolograms

569 Parasites were prepared as for MSF assays. Isobologram design followed the procedure in [78].
570 Serial dilutions were planned so that the $IC_{50}$s of each drug would be in the second two-fold dilution
571 out of 6 total dilutions. $IC_{50}$s for each combination solution were calculated using sigmoidal best-fit
572 curves assigned in Graphpad Prism. Fractional inhibitory concentrations (FIC values) were calculated
573 in Excel [79] and isobolograms plotted in Graphpad Prism. Source data for the isobolograms are
574 provided in figure S8.

## 575 Ring-stage Survival Assay (RSA)

576 Parasite cultures at 8-10% schizonts were synchronised using percoll and Compound 2 as in [62],
577 then allowed to reinvade. Early ring-stage (0-3 hpi) parasites at 0.5% parasitaemia, 2% haematocrit
578 were exposed for 6 h to 700 nM DHA or 0.02% DMSO (vehicle control) under normal conditions,
579 before washing three times with incomplete media, resuspending in complete media and incubating
580 under the same conditions for a further 66 h. In addition to the DHA 700 nM pulse, VE-821 and KU-

581 55933 inhibitors were used at 0.5x $IC_{50}$ with DHA, or by themselves, throughout the 6 h pulse period.
582 72 h after initial drug exposure, 20 µl was frozen for RT-PCR as per eRRSA protocol [55].

## 583 qPCR-based RSA analysis

584 qPCR amplification was used to quantify live parasites in the eRRSA [55]. The Phusion Blood Direct
585 PCR kit was used (ThermoFisher, cat # F547L), supplemented with 1x SYBR Green I (ThermoFisher)
586 and 50 nM Low ROX (ThermoFisher), according to the manufacturer's instructions. qPCR
587 amplification was measured using the fast mode of the ABI 7900HT, with a 20 s denaturation at 95
588 °C, followed by 35 cycles of 95 °C for 1 s, 62.3 °C for 30 s, and 65 °C for 15 s. Cycle threshold (Ct)
589 values were calculated; then the fold change was calculated by determining the mean difference in
590 Ct (ΔCt) for the three technical replicates between the untreated and DHA-treated samples by
591 applying the following equation: Fold change =2^(ΔCt of treated – ΔCt of untreated). This was -log
592 transformed and data were plotted in GraphPad Prism.

## 593 Flow cytometry-based RSA analysis

594 Flow cytometry wash buffer 'FC wash' (2% FBS (Gibco) in HBSS (calcium, magnesium, no phenol red,
595 Gibco) was prepared. The remaining 180 µl of each RSA assay, not harvested for eRRSA, was
596 centrifuged and packed cells were washed three times in 200 µL of FC wash, then resuspended in FC
597 wash to make a 10% haematocrit suspension. 25 µL of suspension from each assay (conducted in
598 technical triplicate) were mixed with 25 µL of 0.6X SYBR Green I (SYBR) with 1.5 nM MitoTracker
599 Deep Red FM (MT, Invitrogen) in FC wash. Compensation controls were prepared with suspension
600 from one DMSO-treated triplicate, labelled with either 0.6X SYBR, 1.5 nM MT, or FC wash alone.
601 Samples were incubated in the dark at 37°C for 30 min, then washed three times in 200 µL and
602 resuspended in 180 µL of FC wash.

603 10,000 events of SYBR positive cells were captured at a flow rate of 25 µL/min on an Attune NxT
604 Acoustic Focusing Cytometer (Invitrogen). SYBR and MT fluorescence were detected on the BL1 (488

605 nm excitation, 530/30 nm emission, 340 V) and RL1 (638 nm excitation, 670/14 nm emission, 510 V)
606 channels respectively. Debris and doublets were excluded by gating on a forward scatter area (FSC-
607 A) versus side scatter height (SSC-H) plot and forward scatter area (FSC-A) versus forward scatter
608 height (FSC-H). SYBR/MT quadrant plots were generated using the Attune NxT software v4.2.0
609 (Invitrogen).

## 610 Antibody production

611 Peptides were designed from *P. falciparum* PI3K (PF3D7_0515300) with help from Eurogentec using
612 parameters such as size, amino acid composition, hydrophobicity and secondary structure. Two
613 peptides were chosen - one predicted to be in the catalytic domain and one upstream of this
614 domain, both predicted to be surface-displayed. N-terminal cysteines were added to the peptide
615 sequences to target the coupling site at the carrier protein.
616 Antibodies were raised by Eurogentec. Two rabbits were bled for pre-immune sera, inoculated with
617 both peptides, then further immunised with 3 booster inoculations at 12 days, ~1 month and
618 ~2months. Immune serum was collected after ~9 weeks.

## 619 Western blotting

620 Parasites were extracted from infected erythrocytes by mixing with 0.5 volumes of 0.2% saponin in
621 PBS and incubating for 10 min on ice. Saponin lysates were centrifuged at 15,000 *xg* at 4 °C for 10
622 min, washed 3 x in ice-cold PBS, centrifuged at 15,000 *xg* for 5 min and resuspended in PBS before
623 freezing at -20°C. Parasites obtained by saponin lysis were resuspended in 1x RIPA buffer (150 mM
624 sodium chloride, 1.0% NP-40 or Triton X-100, 0.5% sodium deoxycholate, 0.1% SDS and 50 mM Tris
625 pH 8) with protease inhibitors (ROCHE, Complete Mini) added directly before use, then freeze-
626 thawed 3 times. Cell debris was removed by centrifugation at 4 °C, 13,000 *xg*, and supernatant was
627 mixed with 1 x NuPage LDS Sample Buffer (ThermoFisher: NP0007), supplemented with 0.1% 2-
628 mercaptoethanol, then boiled at 90 °C for 5 min. Protein lysates were resolved on 4-15% TRIS-

629 glycine gels (BIO-RAD Mini -PROTEAN TGX) for 1–2 h at 100 V in 1X TGS buffer. Wet transfer was
630 completed onto nitrocellulose membrane 0.2-µM-pore-size (Amersham Protran®, GE Healthcare)
631 at 60 V for 45 min.

632 Membranes were blocked with 3% BSA TBST for 1 h, washed once in TBST and incubated overnight
633 in primary antibody diluted in blocking buffer at 4 °C. Blots were washed 3x 5 min in TBST and
634 incubated in a secondary antibody diluted 1:5000 in blocking buffer for 1 h. Blots were washed again
635 (3x 5 min, TBST), developed using SuperSignal West Pico Plus Chemiluminescent Substrate and
636 imaged on a gel imager (Azure, Q500). Some membranes were stripped prior to re-blocking (10 ml
637 20% SDS and 12.5 ml 0.5M Tris HCL, pH 6.8, added to 77.5 ml distilled water, with 0.8 ml β-
638 mercaptoethanol added just before use). 5 ml stripping buffer (warmed to 50 °C) was added to a
639 blot and incubated at 50 °C for 45 min with agitation. The stripping buffer was removed, and the
640 membrane was washed under a running tap for 1-2 min, then washed 3x 5 min with TBST. The
641 membrane was then ready for re-blocking.

642 Antibodies used were pre-immune or immune sera for *Pf*PI3K peptides, diluted 1:200, with
643 secondary goat anti-rabbit HRP 1:5000 (Abcam, ab97080); or rabbit α-γ-H2aX (Cell signalling, 9718S)
644 with goat α-Rabbit IgG (H+L) Cross-Adsorbed Secondary Antibody, Alexa Fluor 594 (Invitrogen, A-
645 11012).

646

647 # Acknowledgements

648 We would like to thank Dr Holly Matthews for early work on this project, Dr Ibtissam Jabre for help
649 with H2A-P blots, Prof Kai Wengelnik for sharing the PI3K inducible knockout line swiftly during
650 revision of this manuscript, and Profs Marcus Lee and Paul Roepe for helpful early discussions.

651 This work was funded by the European Research Council (ERC) under the European Union's Horizon
652 2020 research and innovation programme (ERC-2016-COG 725126 to CJM); and a PhD studentship
653 from the University of Cambridge Department of Pathology to MKJ. The funders had no role in study
654 design, data collection, interpretation or the decision to submit the work for publication.

655

656 # References

657 1. WHO. World Malaria Report 2023. 2023. Epub 2023.
658 2. Klaus S, Binder P, Kim J, Machado M, Funaya C, Schaaf V, et al. Asynchronous nuclear cycles
659 in multinucleated Plasmodium falciparum facilitate rapid proliferation. Sci Adv. 2022;8(13):eabj5362.
660 doi: 10.1126/sciadv.abj5362. PubMed PMID: 35353560.
661 3. McDonald J, Merrick CJ. DNA replication dynamics during erythrocytic schizogony in the
662 malaria parasites Plasmodium falciparum and Plasmodium knowlesi. PLoS pathogens. 2022;18(6):
663 e1010595.
664 4. Simon CS, Sturmer VS, Guizetti J. How Many Is Enough? - Challenges of Multinucleated Cell
665 Division in Malaria Parasites. Front Cell Infect Microbiol. 2021;11:658616. doi:
666 10.3389/fcimb.2021.658616. PubMed PMID: 34026661; PubMed Central PMCID: PMCPMC8137892.
667 5. Liffner B, Cepeda Diaz AK, Blauwkamp J, Anaguano D, Frolich S, Muralidharan V, et al. Atlas
668 of Plasmodium falciparum intraerythrocytic development using expansion microscopy. Elife.
669 2023;12. doi: 10.7554/eLife.88088. PubMed PMID: 38108809; PubMed Central PMCID:
670 PMCPMC10727503.
671 6. Matthews H, Duffy CW, Merrick CJ. Checks and balances? DNA replication and the cell cycle
672 in Plasmodium. Parasit Vectors. 2018;11(1):216. doi: 10.1186/s13071-018-2800-1. PubMed PMID:
673 29587837; PubMed Central PMCID: PMCPMC5872521.
674 7. Zhou BB, Elledge SJ. The DNA damage response: putting checkpoints in perspective. Nature.
675 2000;408(6811):433-9. doi: 10.1038/35044005. PubMed PMID: 11100718.
676 8. Hawkins LM, Naumov AV, Batra M, Wang C, Chaput D, Suvorova ES. Novel CRK-Cyclin
677 Complex Controls Spindle Assembly Checkpoint in Toxoplasma Endodyogeny. mBio.
678 2021;13(1):e0356121. doi: 10.1128/mbio.03561-21. PubMed PMID: 35130726; PubMed Central
679 PMCID: PMCPMC8822342.
680 9. Naumov AV, Wang C, Chaput D, Ting LM, Alvarez CA, Keller T, et al. Restriction Checkpoint
681 Controls Bradyzoite Development in Toxoplasma gondii. Microbiol Spectr. 2022;10(3):e0070222. doi:
682 10.1128/spectrum.00702-22. PubMed PMID: 35652638; PubMed Central PMCID: PMCPMC9241953.
683 10. Alvarez CA, Suvorova ES. Checkpoints of apicomplexan cell division identified in Toxoplasma
684 gondii. PLoS pathogens. 2017;13(7):e1006483. doi: 10.1371/journal.ppat.1006483. PubMed PMID:
685 28671988; PubMed Central PMCID: PMCPMC5510908.
686 11. Lee AH, Symington LS, Fidock DA. DNA repair mechanisms and their biological roles in the
687 malaria parasite Plasmodium falciparum. Microbiol Mol Biol Rev. 2014;78(3):469-86. doi:
688 10.1128/MMBR.00059-13. PubMed PMID: 25184562; PubMed Central PMCID: PMCPMC4187680.
689 12. Claessens A, Hamilton WL, Kekre M, Otto TD, Faizullabhoy A, Rayner JC, et al. Generation of
690 antigenic diversity in Plasmodium falciparum by structured rearrangement of Var genes during
691 mitosis. PLoS genetics. 2014;10(12):e1004812. doi: 10.1371/journal.pgen.1004812. PubMed PMID:
692 25521112; PubMed Central PMCID: PMCPMC4270465.

693 13. Platon L, Menard D. Plasmodium falciparum ring-stage plasticity and drug resistance. Trends
694 Parasitol. 2024;40(2):118-30. doi: 10.1016/j.pt.2023.11.007. PubMed PMID: 38104024.
695 14. Babbitt SE, Altenhofen L, Cobbold SA, Istvan ES, Fennell C, Doerig C, et al. Plasmodium
696 falciparum responds to amino acid starvation by entering into a hibernatory state. Proceedings of
697 the National Academy of Sciences of the United States of America. 2012;109(47):E3278-87. doi:
698 10.1073/pnas.1209823109. PubMed PMID: 23112171; PubMed Central PMCID: PMCPMC3511138.
699 15. Yuan L, Hao M, Wu L, Zhao Z, Rosenthal BM, Li X, et al. Refrigeration provides a simple
700 means to synchronize in vitro cultures of Plasmodium falciparum. Exp Parasitol. 2014;140:18-23. doi:
701 10.1016/j.exppara.2014.03.010. PubMed PMID: 24632190; PubMed Central PMCID:
702 PMCPMC4018460.
703 16. Bohorquez EB, Juliano JJ, Kim HS, Meshnick SR. Mefloquine exposure induces cell cycle delay
704 and reveals stage-specific expression of the pfmdr1 gene. Antimicrobial agents and chemotherapy.
705 2013;57(2):833-9. doi: 10.1128/AAC.01006-12. PubMed PMID: 23208721; PubMed Central PMCID:
706 PMCPMC3553685.
707 17. Witkowski B, Lelievre J, Barragan MJ, Laurent V, Su XZ, Berry A, et al. Increased tolerance to
708 artemisinin in Plasmodium falciparum is mediated by a quiescence mechanism. Antimicrobial agents
709 and chemotherapy. 2010;54(5):1872-7. doi: 10.1128/AAC.01636-09. PubMed PMID: 20160056;
710 PubMed Central PMCID: PMCPMC2863624.
711 18. Gupta DK, Patra AT, Zhu L, Gupta AP, Bozdech Z. DNA damage regulation and its role in drug-
712 related phenotypes in the malaria parasites. Sci Rep. 2016;6:23603. doi: 10.1038/srep23603.
713 PubMed PMID: 27033103; PubMed Central PMCID: PMCPMC4817041.
714 19. Voss Y, Klaus S, Guizetti J, Ganter M. Plasmodium schizogony, a chronology of the parasite's
715 cell cycle in the blood stage. PLoS pathogens. 2023;19(3):e1011157. doi:
716 10.1371/journal.ppat.1011157. PubMed PMID: 36862652; PubMed Central PMCID:
717 PMCPMC9980825 commercial or financial relationships that could be construed as a potential
718 conflict of interest.
719 20. Absalon S, Dvorin JD. Depletion of the mini-chromosome maintenance complex binding
720 protein allows the progression of cytokinesis despite abnormal karyokinesis during the asexual
721 development of Plasmodium falciparum. Cellular microbiology. 2021;23(3):e13284. doi:
722 10.1111/cmi.13284. PubMed PMID: 33124706; PubMed Central PMCID: PMCPMC8058698.
723 21. Janse CJ, van der Klooster PF, van der Kaay HJ, van der Ploeg M, Overdulve JP. DNA synthesis
724 in Plasmodium berghei during asexual and sexual development. Molecular and biochemical
725 parasitology. 1986;20(2):173-82. doi: 10.1016/0166-6851(86)90029-0. PubMed PMID: 3092048.
726 22. Matthews H, McDonald J, Totanes FIG, Merrick CJ. Dynamics of DNA replication during male
727 gametogenesis in the malaria parasite Plasmodium falciparum. Cellular microbiology. 2022. doi:
728 doi.org/10.1101/2021.12.18.473304
729 23. Merrick CJ, Jackson D, Diffley JF. Visualization of altered replication dynamics after DNA
730 damage in human cells. The Journal of biological chemistry. 2004;279(19):20067-75. PubMed PMID:
731 14982920.
732 24. Santocanale C, Diffley JF. A Mec1- and Rad53-dependent checkpoint controls late-firing
733 origins of DNA replication. Nature. 1998;395(6702):615-8. doi: 10.1038/27001. PubMed PMID:
734 9783589.
735 25. Goyal M, Heinberg A, Mitesser V, Kandelis-Shalev S, Singh BK, Dzikowski R. Phosphorylation
736 of the Canonical Histone H2A Marks Foci of Damaged DNA in Malaria Parasites. mSphere. 2021;6(1).
737 doi: 10.1128/mSphere.01131-20. PubMed PMID: 33441412; PubMed Central PMCID:
738 PMCPMC7845613.
739 26. Helt CE, Cliby WA, Keng PC, Bambara RA, O'Reilly MA. Ataxia telangiectasia mutated (ATM)
740 and ATM and Rad3-related protein exhibit selective target specificities in response to different forms
741 of DNA damage. The Journal of biological chemistry. 2005;280(2):1186-92. doi:
742 10.1074/jbc.M410873200. PubMed PMID: 15533933.

743 27. Rogakou EP, Pilch DR, Orr AH, Ivanova VS, Bonner WM. DNA double-stranded breaks induce
744 histone H2AX phosphorylation on serine 139. The Journal of biological chemistry.
745 1998;273(10):5858-68. doi: 10.1074/jbc.273.10.5858. PubMed PMID: 9488723.
746 28. Beranek DT. Distribution of methyl and ethyl adducts following alkylation with
747 monofunctional alkylating agents. Mutat Res. 1990;231(1):11-30. doi: 10.1016/0027-5107(90)90173-
748 2. PubMed PMID: 2195323.
749 29. Gopalakrishnan AM, Kumar N. Opposing roles for two molecular forms of replication protein
750 A in Rad51-Rad54-mediated DNA recombination in Plasmodium falciparum. mBio.
751 2013;4(3):e00252-13. doi: 10.1128/mBio.00252-13. PubMed PMID: 23631919; PubMed Central
752 PMCID: PMCPMC3648904.
753 30. Craven HM, Nettesheim G, Cicuta P, Blagborough AM, Merrick CJ. Effects of the G-
754 quadruplex-binding drugs quarfloxin and CX-5461 on the malaria parasite Plasmodium falciparum.
755 Int J Parasitol Drugs Drug Resist. 2023;23:106-19. doi: 10.1016/j.ijpddr.2023.11.007. PubMed PMID:
756 38041930; PubMed Central PMCID: PMCPMC10711401.
757 31. Hassett MR, Roepe PD. PIK-ing New Malaria Chemotherapy. Trends Parasitol.
758 2018;34(11):925-7. doi: 10.1016/j.pt.2018.06.003. PubMed PMID: 29934102.
759 32. Mbengue A, Bhattacharjee S, Pandharkar T, Liu H, Estiu G, Stahelin RV, et al. A molecular
760 mechanism of artemisinin resistance in Plasmodium falciparum malaria. Nature.
761 2015;520(7549):683-7. doi: 10.1038/nature14412. PubMed PMID: 25874676; PubMed Central
762 PMCID: PMCPMC4417027.
763 33. Hoang DT, Chernomor O, von Haeseler A, Minh BQ, Vinh LS. UFBoot2: Improving the
764 Ultrafast Bootstrap Approximation. Mol Biol Evol. 2018;35(2):518-22. doi: 10.1093/molbev/msx281.
765 PubMed PMID: 29077904; PubMed Central PMCID: PMCPMC5850222.
766 34. Hassett MR, Sternberg AR, Riegel BE, Thomas CJ, Roepe PD. Heterologous Expression,
767 Purification, and Functional Analysis of Plasmodium falciparum Phosphatidylinositol 3'-Kinase.
768 Biochemistry. 2017;56(33):4335-45. doi: 10.1021/acs.biochem.7b00416. PubMed PMID: 28719180.
769 35. Tawk L, Chicanne G, Dubremetz JF, Richard V, Payrastre B, Vial HJ, et al. Phosphatidylinositol
770 3-phosphate, an essential lipid in Plasmodium, localizes to the food vacuole membrane and the
771 apicoplast. Eukaryotic cell. 2010;9(10):1519-30. doi: 10.1128/EC.00124-10. PubMed PMID:
772 20709789; PubMed Central PMCID: PMCPMC2950420.
773 36. Vaid A, Ranjan R, Smythe WA, Hoppe HC, Sharma P. PfPI3K, a phosphatidylinositol-3 kinase
774 from Plasmodium falciparum, is exported to the host erythrocyte and is involved in hemoglobin
775 trafficking. Blood. 2010;115(12):2500-7. doi: 10.1182/blood-2009-08-238972. PubMed PMID:
776 20093402; PubMed Central PMCID: PMCPMC2918364.
777 37. Thomas D, Powell JA, Green BD, Barry EF, Ma Y, Woodcock J, et al. Protein kinase activity of
778 phosphoinositide 3-kinase regulates cytokine-dependent cell survival. PLoS biology.
779 2013;11(3):e1001515. doi: 10.1371/journal.pbio.1001515. PubMed PMID: 23526884; PubMed
780 Central PMCID: PMCPMC3601961.
781 38. Foukas LC, Shepherd PR. Phosphoinositide 3-kinase: the protein kinase that time forgot.
782 Biochem Soc Trans. 2004;32(Pt 2):330-1. doi: 10.1042/bst0320330. PubMed PMID: 15046601.
783 39. Johnson MK, Chelaghma S, Koreny L, Waller RF, Merrick CJ. Characterisation of cell cycle
784 checkpoint kinases in Toxoplasma gondii. BioRxiv. 2024:doi.org/10.1101/2024.09.10.612042. doi:
785 doi.org/10.1101/2024.09.10.612042;.
786 40. Arendse LB, Murithi JM, Qahash T, Pasaje CFA, Godoy LC, Dey S, et al. The anticancer human
787 mTOR inhibitor sapanisertib potently inhibits multiple Plasmodium kinases and life cycle stages. Sci
788 Transl Med. 2022;14(667):eabo7219. doi: 10.1126/scitranslmed.abo7219. PubMed PMID: 36260689;
789 PubMed Central PMCID: PMCPMC9951552.
790 41. Mukherjee A, Crochetiere ME, Sergerie A, Amiar S, Thompson LA, Ebrahimzadeh Z, et al. A
791 Phosphoinositide-Binding Protein Acts in the Trafficking Pathway of Hemoglobin in the Malaria
792 Parasite Plasmodium falciparum. mBio. 2022;13(1):e0323921. doi: 10.1128/mbio.03239-21. PubMed
793 PMID: 35038916; PubMed Central PMCID: PMCPMC8764524.

794 42. Oehring SC, Woodcroft BJ, Moes S, Wetzel J, Dietz O, Pulfer A, et al. Organellar proteomics
795 reveals hundreds of novel nuclear proteins in the malaria parasite Plasmodium falciparum. Genome
796 biology. 2012;13(11):R108. doi: 10.1186/gb-2012-13-11-r108. PubMed PMID: 23181666; PubMed
797 Central PMCID: PMCPMC4053738.
798 43. Briquet S, Ourimi A, Pionneau C, Bernardes J, Carbone A, Chardonnet S, et al. Identification
799 of Plasmodium falciparum nuclear proteins by mass spectrometry and proposed protein annotation.
800 PloS one. 2018;13(10):e0205596. doi: 10.1371/journal.pone.0205596. PubMed PMID: 30379851;
801 PubMed Central PMCID: PMCPMC6209197.
802 44. Barylyuk K, Koreny L, Ke H, Butterworth S, Crook OM, Lassadi I, et al. A Comprehensive
803 Subcellular Atlas of the Toxoplasma Proteome via hyperLOPIT Provides Spatial Context for Protein
804 Functions. Cell host & microbe. 2020;28(5):752-66 e9. doi: 10.1016/j.chom.2020.09.011. PubMed
805 PMID: 33053376; PubMed Central PMCID: PMCPMC7670262.
806 45. Birnbaum J, Scharf S, Schmidt S, Jonscher E, Hoeijmakers WAM, Flemming S, et al. A Kelch13-
807 defined endocytosis pathway mediates artemisinin resistance in malaria parasites. Science (New
808 York, NY. 2020;367(6473):51-9. doi: 10.1126/science.aax4735. PubMed PMID: 31896710.
809 46. Reaper PM, Griffiths MR, Long JM, Charrier JD, Maccormick S, Charlton PA, et al. Selective
810 killing of ATM- or p53-deficient cancer cells through inhibition of ATR. Nat Chem Biol. 2011;7(7):428-
811 30. doi: 10.1038/nchembio.573. PubMed PMID: 21490603.
812 47. Hickson I, Zhao Y, Richardson CJ, Green SJ, Martin NM, Orr AI, et al. Identification and
813 characterization of a novel and specific inhibitor of the ataxia-telangiectasia mutated kinase ATM.
814 Cancer research. 2004;64(24):9152-9. doi: 10.1158/0008-5472.CAN-04-2727. PubMed PMID:
815 15604286.
816 48. Safeukui I, Ware RE, Mohandas N, Haldar K. Simultaneous adjunctive treatment of malaria
817 and its coevolved genetic disorder sickle cell anemia. Blood Adv. 2023;7(19):5970-81. doi:
818 10.1182/bloodadvances.2022009124. PubMed PMID: 37093647; PubMed Central PMCID:
819 PMCPMC10580175 interests.
820 49. Al Monla R, Penzo M, Vallentin A, Lohia R, Vincent J, Berry L, et al. PI3-kinase has multiple
821 functions in asexual blood stages of Plasmodium falciparum. Sci Rep. 2025;15(1):16762. doi:
822 10.1038/s41598-025-01397-1. PubMed PMID: 40369090; PubMed Central PMCID:
823 PMCPMC12078608.
824 50. Bower-Lepts C, Rawat M, Keith WC, Girling G, Luth MR, Carolino K, et al. A novel
825 chemogenomic screening platform for scalable antimalarial drug target identification. bioRxiv.
826 2024:2024.08.27.609875. doi: 10.1101/2024.08.27.609875.
827 51. Ismail HM, Barton V, Phanchana M, Charoensutthivarakul S, Wong MH, Hemingway J, et al.
828 Artemisinin activity-based probes identify multiple molecular targets within the asexual stage of the
829 malaria parasites Plasmodium falciparum 3D7. Proceedings of the National Academy of Sciences of
830 the United States of America. 2016;113(8):2080-5. doi: 10.1073/pnas.1600459113. PubMed PMID:
831 26858419; PubMed Central PMCID: PMCPMC4776496.
832 52. Xiong A, Prakash P, Gao X, Chew M, Tay IJJ, Woodrow CJ, et al. K13-Mediated Reduced
833 Susceptibility to Artemisinin in Plasmodium falciparum Is Overlaid on a Trait of Enhanced DNA
834 Damage Repair. Cell Rep. 2020;32(5):107996. doi: 10.1016/j.celrep.2020.107996. PubMed PMID:
835 32755588; PubMed Central PMCID: PMCPMC7408483.
836 53. Gopalakrishnan AM, Kumar N. Antimalarial action of artesunate involves DNA damage
837 mediated by reactive oxygen species. Antimicrobial agents and chemotherapy. 2015;59(1):317-25.
838 doi: 10.1128/AAC.03663-14. PubMed PMID: 25348537; PubMed Central PMCID: PMCPMC4291367.
839 54. Straimer J, Gnadig NF, Witkowski B, Amaratunga C, Duru V, Ramadani AP, et al. Drug
840 resistance. K13-propeller mutations confer artemisinin resistance in Plasmodium falciparum clinical
841 isolates. Science (New York, NY. 2015;347(6220):428-31. doi: 10.1126/science.1260867. PubMed
842 PMID: 25502314; PubMed Central PMCID: PMCPMC4349400.
843 55. Davis SZ, Singh PP, Vendrely KM, Shoue DA, Checkley LA, McDew-White M, et al. The
844 extended recovery ring-stage survival assay provides a superior association with patient clearance

845 half-life and increases throughput. Malaria journal. 2020;19(1):54. doi: 10.1186/s12936-020-3139-6.
846 PubMed PMID: 32005233; PubMed Central PMCID: PMCPMC6995136.
847 56. Merrick CJ. Transfection with thymidine kinase permits bromodeoxyuridine labelling of DNA
848 replication in the human malaria parasite Plasmodium falciparum. Malar J. 2015;14(490). doi:
849 10.1186/s12936-015-1014-7.
850 57. Courtot L, Hoffmann JS, Bergoglio V. The Protective Role of Dormant Origins in Response to
851 Replicative Stress. Int J Mol Sci. 2018;19(11). doi: 10.3390/ijms19113569. PubMed PMID: 30424570;
852 PubMed Central PMCID: PMCPMC6274952.
853 58. Mott BT, Eastman RT, Guha R, Sherlach KS, Siriwardana A, Shinn P, et al. High-throughput
854 matrix screening identifies synergistic and antagonistic antimalarial drug combinations. Sci Rep.
855 2015;5:13891. doi: 10.1038/srep13891. PubMed PMID: 26403635; PubMed Central PMCID:
856 PMCPMC4585899.
857 59. Nardella F, Jiang T, Wang L, Bohmer MJ, Chakraborty S, Okombo J, et al.
858 Plasmodiumfalciparum protein kinase 6 and hemozoin formation are inhibited by a type II human
859 kinase inhibitor exhibiting antimalarial activity. Cell Chem Biol. 2025;32(7):926-41 e23. doi:
860 10.1016/j.chembiol.2025.06.003. PubMed PMID: 40628257.
861 60. Ward P, Equinet L, Packer J, Doerig C. Protein kinases of the human malaria parasite
862 Plasmodium falciparum: the kinome of a divergent eukaryote. BMC genomics. 2004;5:79. doi:
863 10.1186/1471-2164-5-79. PubMed PMID: 15479470; PubMed Central PMCID: PMCPMC526369.
864 61. Ganter M, Goldberg JM, Dvorin JD, Paulo JA, King JG, Tripathi AK, et al. Plasmodium
865 falciparum CRK4 directs continuous rounds of DNA replication during schizogony. Nat Microbiol.
866 2017;2:17017. doi: 10.1038/nmicrobiol.2017.17. PubMed PMID: 28211852; PubMed Central PMCID:
867 PMCPMC5328244.
868 62. Totanes FIG, Gockel J, Chapman SE, Bartfai R, Boemo MA, Merrick CJ. A genome-wide map
869 of DNA replication at single-molecule resolution in the malaria parasite Plasmodium falciparum.
870 Nucleic acids research. 2023. doi: 10.1093/nar/gkad093. PubMed PMID: 36808528.
871 63. Lewis WH, Paris G, Beedessee G, Koreny L, Flores V, Dendooven T, et al. Plastid translocon
872 recycling in dinoflagellates demonstrates the portability of complex plastids between hosts. Curr
873 Biol. 2024;34(23):5494-506 e3. doi: 10.1016/j.cub.2024.10.034. PubMed PMID: 39571577; PubMed
874 Central PMCID: PMCPMC7617431.
875 64. UniProt C. UniProt: the Universal Protein Knowledgebase in 2023. Nucleic acids research.
876 2023;51(D1):D523-D31. doi: 10.1093/nar/gkac1052. PubMed PMID: 36408920; PubMed Central
877 PMCID: PMCPMC9825514.
878 65. Keeling PJ, Burki F, Wilcox HM, Allam B, Allen EE, Amaral-Zettler LA, et al. The Marine
879 Microbial Eukaryote Transcriptome Sequencing Project (MMETSP): illuminating the functional
880 diversity of eukaryotic life in the oceans through transcriptome sequencing. PLoS biology.
881 2014;12(6):e1001889. doi: 10.1371/journal.pbio.1001889. PubMed PMID: 24959919; PubMed
882 Central PMCID: PMCPMC4068987.
883 66. Alvarez-Jarreta J, Amos B, Aurrecoechea C, Bah S, Barba M, Barreto A, et al. VEuPathDB: the
884 eukaryotic pathogen, vector and host bioinformatics resource center in 2023. Nucleic acids research.
885 2024;52(D1):D808-D16. doi: 10.1093/nar/gkad1003. PubMed PMID: 37953350; PubMed Central
886 PMCID: PMCPMC10767879.
887 67. Mathur V, Kolisko M, Hehenberger E, Irwin NAT, Leander BS, Kristmundsson A, et al.
888 Multiple Independent Origins of Apicomplexan-Like Parasites. Curr Biol. 2019;29(17):2936-41 e5.
889 doi: 10.1016/j.cub.2019.07.019. PubMed PMID: 31422883.
890 68. Janouskovec J, Paskerova GG, Miroliubova TS, Mikhailov KV, Birley T, Aleoshin VV, et al.
891 Apicomplexan-like parasites are polyphyletic and widely but selectively dependent on cryptic plastid
892 organelles. Elife. 2019;8. doi: 10.7554/eLife.49662. PubMed PMID: 31418692; PubMed Central
893 PMCID: PMCPMC6733595.

894 69. Camacho C, Coulouris G, Avagyan V, Ma N, Papadopoulos J, Bealer K, et al. BLAST+:
895 architecture and applications. BMC bioinformatics. 2009;10:421. doi: 10.1186/1471-2105-10-421.
896 PubMed PMID: 20003500; PubMed Central PMCID: PMCPMC2803857.
897 70. Fu L, Niu B, Zhu Z, Wu S, Li W. CD-HIT: accelerated for clustering the next-generation
898 sequencing data. Bioinformatics. 2012;28(23):3150-2. doi: 10.1093/bioinformatics/bts565. PubMed
899 PMID: 23060610; PubMed Central PMCID: PMCPMC3516142.
900 71. Katoh K, Standley DM. MAFFT multiple sequence alignment software version 7:
901 improvements in performance and usability. Mol Biol Evol. 2013;30(4):772-80. doi:
902 10.1093/molbev/mst010. PubMed PMID: 23329690; PubMed Central PMCID: PMCPMC3603318.
903 72. Capella-Gutierrez S, Silla-Martinez JM, Gabaldon T. trimAl: a tool for automated alignment
904 trimming in large-scale phylogenetic analyses. Bioinformatics. 2009;25(15):1972-3. doi:
905 10.1093/bioinformatics/btp348. PubMed PMID: 19505945; PubMed Central PMCID:
906 PMCPMC2712344.
907 73. Price MN, Dehal PS, Arkin AP. FastTree 2--approximately maximum-likelihood trees for large
908 alignments. PloS one. 2010;5(3):e9490. doi: 10.1371/journal.pone.0009490. PubMed PMID:
909 20224823; PubMed Central PMCID: PMCPMC2835736.
910 74. Minh BQ, Schmidt HA, Chernomor O, Schrempf D, Woodhams MD, von Haeseler A, et al. IQ-
911 TREE 2: New Models and Efficient Methods for Phylogenetic Inference in the Genomic Era. Mol Biol
912 Evol. 2020;37(5):1530-4. doi: 10.1093/molbev/msaa015. PubMed PMID: 32011700; PubMed Central
913 PMCID: PMCPMC7182206.
914 75. Gu X, Fu YX, Li WH. Maximum likelihood estimation of the heterogeneity of substitution rate
915 among nucleotide sites. Mol Biol Evol. 1995;12(4):546-57. doi:
916 10.1093/oxfordjournals.molbev.a040235. PubMed PMID: 7659011.
917 76. Kalyaanamoorthy S, Minh BQ, Wong TKF, von Haeseler A, Jermiin LS. ModelFinder: fast
918 model selection for accurate phylogenetic estimates. Nature methods. 2017;14(6):587-9. doi:
919 10.1038/nmeth.4285. PubMed PMID: 28481363; PubMed Central PMCID: PMCPMC5453245.
920 77. Smilkstein M, Sriwilaijaroen N, Kelly JX, Wilairat P, Riscoe M. Simple and inexpensive
921 fluorescence-based technique for high-throughput antimalarial drug screening. Antimicrobial agents
922 and chemotherapy. 2004;48(5):1803-6. PubMed PMID: 15105138; PubMed Central PMCID:
923 PMCPMC400546.
924 78. Huang RY, Pei L, Liu Q, Chen S, Dou H, Shu G, et al. Isobologram Analysis: A Comprehensive
925 Review of Methodology and Current Research. Front Pharmacol. 2019;10:1222. doi:
926 10.3389/fphar.2019.01222. PubMed PMID: 31736746; PubMed Central PMCID: PMCPMC6830115.
927 79. Fivelman QL, Adagu IS, Warhurst DC. Modified fixed-ratio isobologram method for studying
928 in vitro interactions between atovaquone and proguanil or dihydroartemisinin against drug-resistant
929 strains of Plasmodium falciparum. Antimicrobial agents and chemotherapy. 2004;48(11):4097-102.
930 doi: 10.1128/AAC.48.11.4097-4102.2004. PubMed PMID: 15504827; PubMed Central PMCID:
931 PMCPMC525430.
932 80. Yang J, Yan R, Roy A, Xu D, Poisson J, Zhang Y. The I-TASSER Suite: protein structure and
933 function prediction. Nature methods. 2015;12(1):7-8. doi: 10.1038/nmeth.3213. PubMed PMID:
934 25549265; PubMed Central PMCID: PMCPMC4428668.

935

# 936 Supporting information

937 **Fig S1: Growth curves determining $IC_{50}$ values for MMS, VE-821 and KU-55933 in the parasite**

938 **strains 3D7, MRA-1252 and MRC-1240.**

939 Each panel shows growth curves from 3-5 independent malaria SYBR green I-based fluorescence
940 (MSF) assays: percentage parasite growth is plotted as a function of drug concentration; error bars
941 are standard errors of the means.

942 A. Inhibition of growth of 3D7 strain by MMS.

943 B. $IC_{50}$ values from the growth curves shown in main figure 3A.

944 C. Inhibition of strains MRA-1252 and MRA-1240 by the drugs VE-821, KU55933 and MMS.

945

946 **Fig S2: 3D7 parasites survive a short pulse of MMS or DHA at the trophozoite stage, but their**
947 **maturation is delayed and progeny number per schizont, reduced.**

948 A. Images were taken 12h after trophozoites at 30-32hpi had been exposed to a 1 h pulse of
949 10X $IC_{50}$ MMS or DHA (2 independent experiments, '1' and '2'). Images show that at this
950 timepoint (i.e. 42-44hpi), cultures were dominated by a mixture of immature and mature
951 schizonts, without clear evidence of parasite death in the damaged cultures. Parasites were
952 then treated with 75nM ML10 for 10 h, to arrest mature schizonts before egress, and re-
953 imaged. Mature schizonts then dominated in all cultures.

954 B. Parasite stages imaged in (A) were categorised as either: early rings, small rings, large rings,
955 early trophozoites, mid trophozoites, late trophozoites, immature schizonts or mature
956 schizonts (2 independent experiments, n ≥ 100 from each experiment). Differences between
957 the proportions of stages in control vs DHA-treated vs MMS-treated cultures were tested via
958 two-way ANOVA and posthoc Tukey's multiple comparisons test. P-values are shown in a
959 table below the graph: *, <0.05; **, <0.01; ***, <0.001. Stars of matched colours across
960 rows denote a significant difference between those conditions (e.g. at 44hpi, there were still
961 more immature schizonts after MMS treatment than in the control (pink stars); 10h later,
962 this difference disappeared, with more mature and fewer immature schizonts (denoted by

963 pairs of yellow and blue stars). The only other difference was in the small numbers of rings
964 that escaped and reinvaded after prolonged arrest.
965 C. Merozoites per schizont were counted in each of the cultures shown in (A) (n = 26-30 per
966 culture). Numbers of merozoites substantially increased in all cultures after the long ML10-
967 arrest period, which allowed mature schizonts to accumulate even after the damage-
968 induced delay seen in (B). A reduction in merozoite number was, however, still seen after
969 MMS damage, although this was not significant after DHA damage.

970

971 **Fig S3: Protein sequence alignment of *P. falciparum* PI3K, PI4K and PIKKs from *S. cerevisiae* and**
972 **human.**

973 A. MUSCLE (3.8) alignment of catalytic domains of *P. falciparum* PI3K and PI4K against human
974 ATM, ATR, PI3K, and yeast Mec1 and Tel1. Colour key is ClustalW standard. Highlighted in
975 the yellow boxes are the catalytic loops in ATR and ATM. Percentage identity matrix is
976 shown below the alignment.

977

978 **Fig S4: Anti-PfPI3K antibody production**

979 A. Model made in i-TASSER [80], threading 1500 C-terminal residues of the 2133-amino acid
980 *Pf*PI3K against human ATR. Protein coloured blue to red, N-terminal to C-terminal. Peptides
981 used as antigens are highlighted in white and circled: amino acids 1359-1374 and 2011-2025
982 of full length *Pf*PI3K.
983 B. Controls for specificity of immune versus pre-immune antisera against *Pf*PI3K.
984 Representative images of single cells are shown. Scale bar 1 µm. Primary antibodies used
985 were rabbit antisera, pre-immune or immune, diluted 1:200 in 3% BSA.

986

987 **Fig S5: Isobolograms showing that two antibiotic drugs do not synergise with MMS**

988 Isobolograms plotted as fractional inhibitory concentrations (FIC) of combinations of MMS and
989 geneticin (G-418), or blasticidin (BSD), as determined by MSF assay. Data were processed as in Figure
990 4B. The type of relationship was defined as additive for blasticidin and borderline antagonistic for
991 geneticin, based on well-established criteria (∑FIC <0.5, substantial synergism; ∑FIC <1, moderate
992 synergism; ∑FIC ≥1 and <2, additive interaction; ∑FIC ≥2 and <4, slight antagonism and ∑FIC >4,
993 marked antagonism).

994

995 **Fig S6: Growth curves determining $IC_{50}$ values for VE-821 and KU-55933 when PI3K is knocked out**

996 A. Example growth curves from malaria SYBR green I-based fluorescence (MSF) assays
997 conducted on the iPI3K-ko line. (As in figure S1, percentage parasite growth is plotted as a
998 function of drug concentration; error bars are standard errors of the means.) Ring-stage
999 parasites of the iPI3K-ko line were treated with 100nM rapamycin to induce gene deletion,
1000 or with DMSO vehicle for the control. MSF assays with VE-821 and KU-55933 were set up
1001 24h later, with drug exposure over 48h, i.e. from trophozoites in cycle-1 to trophozoites in
1002 cycle-2. At 72h, when assays were read, morphology of knockout parasites did not appear
1003 overtly unhealthy. However, if assays were extended to 96h (after reinvasion to cycle-3), all
1004 rapamycin-treated parasites appeared dead, whereas control parasites still appeared
1005 healthy. This delayed-death phenotype precluded any meaningful results from 3-day (72h)
1006 MSF assays, so exclusively 48h assays are shown here.
1007 B. $IC_{50}$ values from the growth curves shown A, and from 3 further replicate assays conducted
1008 on knockout parasites over the same 2-day window (24-72h post-rapamycin). Mean $IC_{50}$s
1009 did not differ markedly from those of the control, nor from those of the 3D7 parent line
1010 (shown in figure S1).

1011

1012 **Fig S7: Ring stage survival assessed by flow cytometry**

1013 A ring-stage survival assay was assessed by flow cytometry as well as eRRSA as used in Figure 5.

1014 Density plot quadrant graphs show one biological replicate of an RSA conducted on 3D7. Cell counts

1015 for each quadrant are shown. Percentage survival was calculated as the proportion of live versus

1016 dead cells (SYBR+ MITO+/SYBR+ MITO-) for each condition.

1017

1018 **Fig S8: Raw growth-curve data for all isobolograms plotted in figures 4B, 5C and S5**

1019 A. Data for isobolgrams in figure 4B, VE-821 with MMS

1020 B. Data for isobolgrams in figure 4B, KU-55933 with MMS

1021 C. Data for isobolgrams in figure 5C, VE-821 and KU55933 with DHA

1022 D. Data for isobolgrams in figure S5, Blasticidin and G-418 with MMS

1023

1024 **Source data files and spreadsheets 1-7:**

1025 Files 1-6: Source data for phylogenetic tree shown in figure 2

1026 Spreadsheet 7: Source data for all other figures and supplementary figures

1027

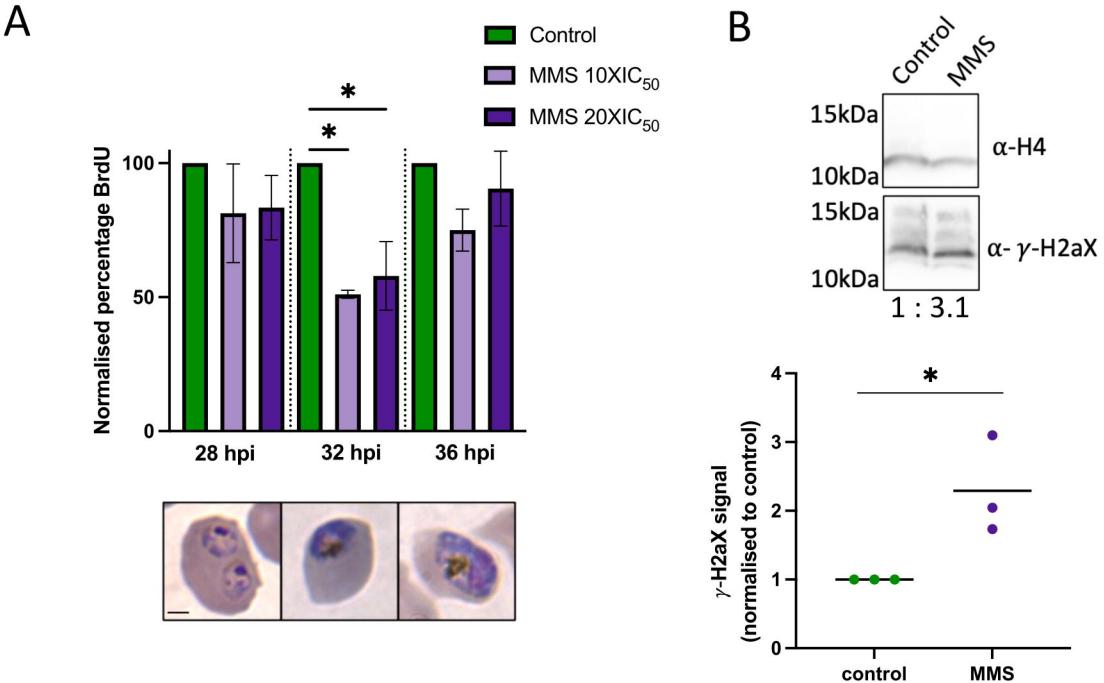
A
Control
MMS 10XIC50
MMS 20XIC50
*
*
Normalised percentage BrdU
100
50
0
28 hpi
32 hpi
36 hpi
B
Control
MMS
15kDa
10kDa
α-H4
15kDa
10kDa
α- γ-H2aX
1 : 3.1
*
γ-H2aX signal
(normalised to control)
4
3
2
1
0
control
MMS

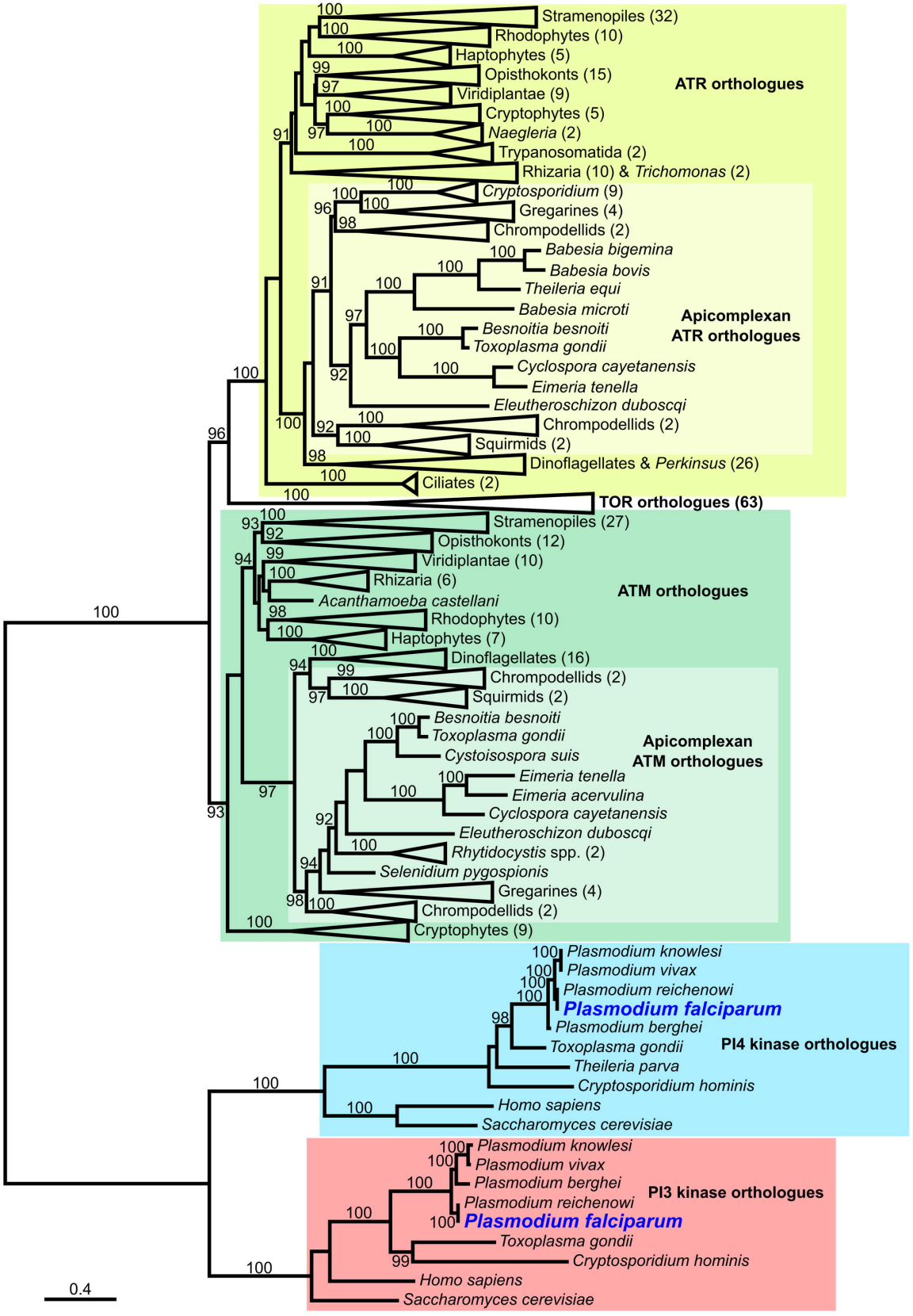
ATR orthologues
Stramenopiles (32)
Rhodophytes (10)
Haptophytes (5)
Opisthokonts (15)
Viridiplantae (9)
Cryptophytes (5)
Naegleria (2)
Trypanosomatida (2)
Rhizaria (10) & Trichomonas (2)
Cryptosporidium (9)
Gregarines (4)
Chrompodellids (2)
Apicomplexan ATR orthologues
Babesia bigemina
Babesia bovis
Theileria equi
Babesia microti
Besnoitia besnoiti
Toxoplasma gondii
Cyclospora cayetanensis
Eimeria tenella
Eleutheroschizon duboscqi
Chrompodellids (2)
Squirmids (2)
Dinoflagellates & Perkinsus (26)
Ciliates (2)
TOR orthologues (63)
ATM orthologues
Stramenopiles (27)
Opisthokonts (12)
Viridiplantae (10)
Rhizaria (6)
Acanthamoeba castellani
Rhodophytes (10)
Haptophytes (7)
Dinoflagellates (16)
Chrompodellids (2)
Squirmids (2)
Apicomplexan ATM orthologues
Besnoitia besnoiti
Toxoplasma gondii
Cystoisospora suis
Eimeria tenella
Eimeria acervulina
Cyclospora cayetanensis
Eleutheroschizon duboscqi
Rhytidocystis spp. (2)
Selenidium pygospionis
Gregarines (4)
Chrompodellids (2)
Cryptophytes (9)
PI4 kinase orthologues
Plasmodium knowlesi
Plasmodium vivax
Plasmodium reichenowi
Plasmodium falciparum
Plasmodium berghei
Toxoplasma gondii
Theileria parva
Cryptosporidium hominis
Homo sapiens
Saccharomyces cerevisiae
PI3 kinase orthologues
Plasmodium knowlesi
Plasmodium vivax
Plasmodium berghei
Plasmodium reichenowi
Plasmodium falciparum
Toxoplasma gondii
Cryptosporidium hominis
Homo sapiens
Saccharomyces cerevisiae
0.4

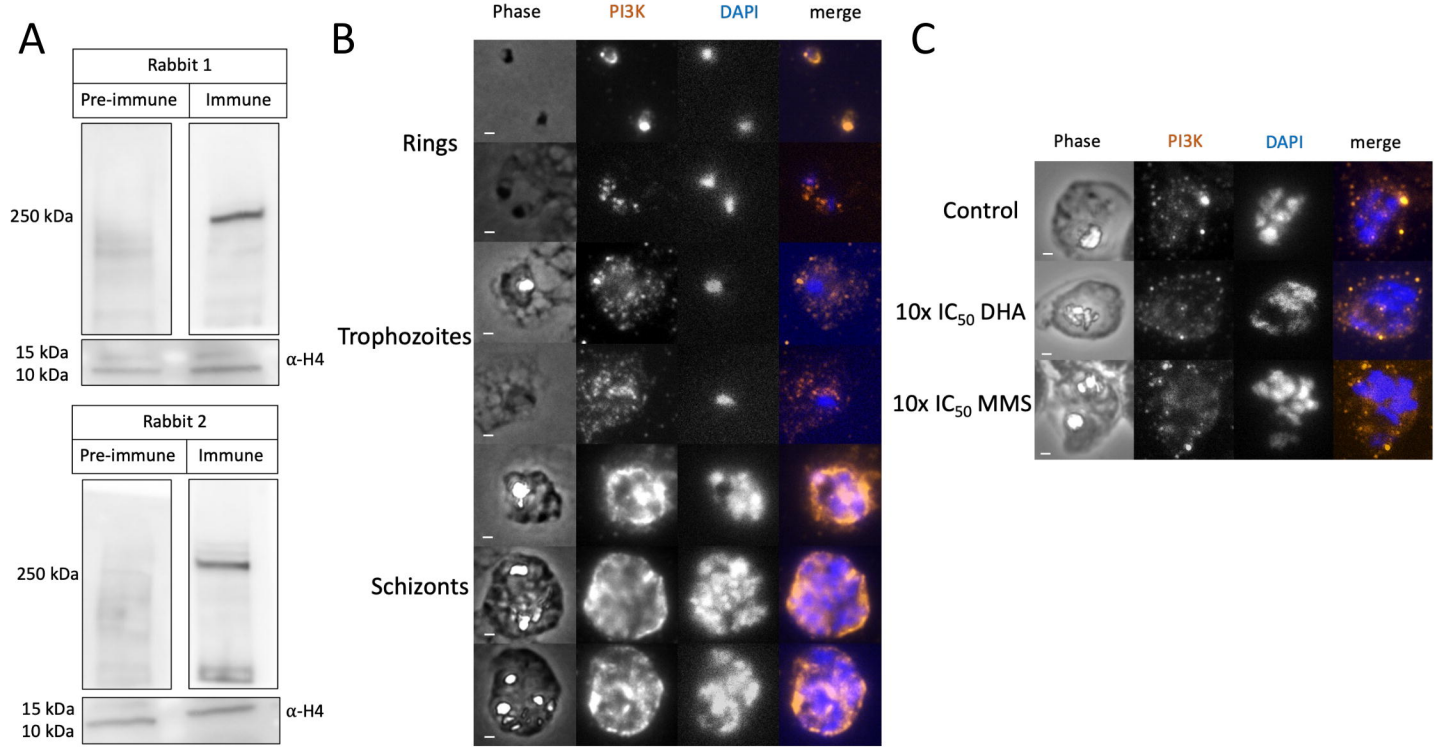
A
Rabbit 1
Pre-immune
Immune
250 kDa
15 kDa
10 kDa
α-H4
Rabbit 2
Pre-immune
Immune
250 kDa
15 kDa
10 kDa
α-H4
B
Phase
PI3K
DAPI
merge
Rings
Trophozoites
Schizonts
C
Phase
PI3K
DAPI
merge
Control
10x IC50 DHA
10x IC50 MMS

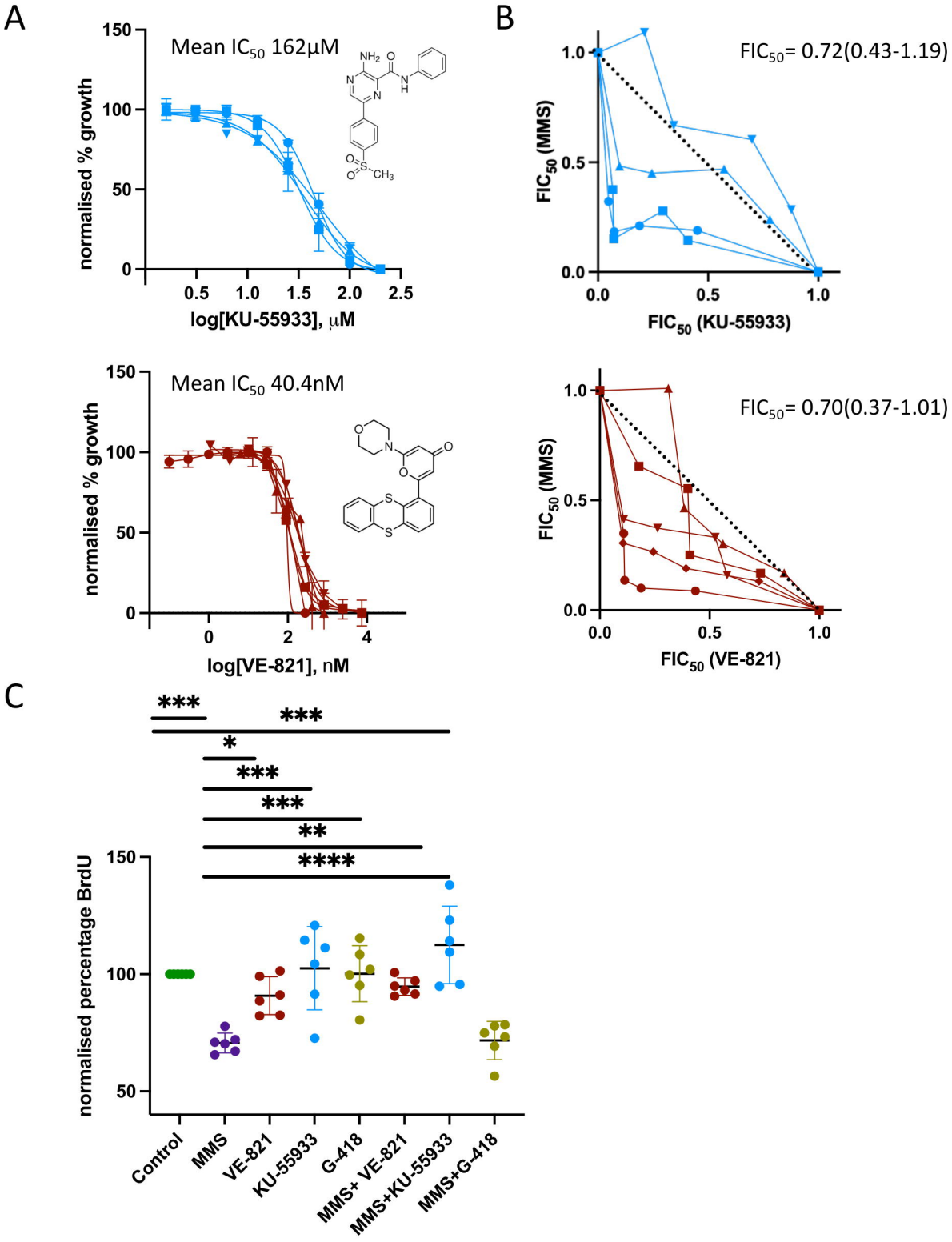
A
Mean IC50 162µM
normalised % growth
log[KU-55933], µM
B
FIC50= 0.72(0.43-1.19)
FIC50 (MMS)
FIC50 (KU-55933)
Mean IC50 40.4nM
normalised % growth
log[VE-821], nM
FIC50= 0.70(0.37-1.01)
FIC50 (MMS)
FIC50 (VE-821)
C
normalised percentage BrdU
Control
MMS
VE-821
KU-55933
G-418
MMS+ VE-821
MMS+KU-55933
MMS+G-418

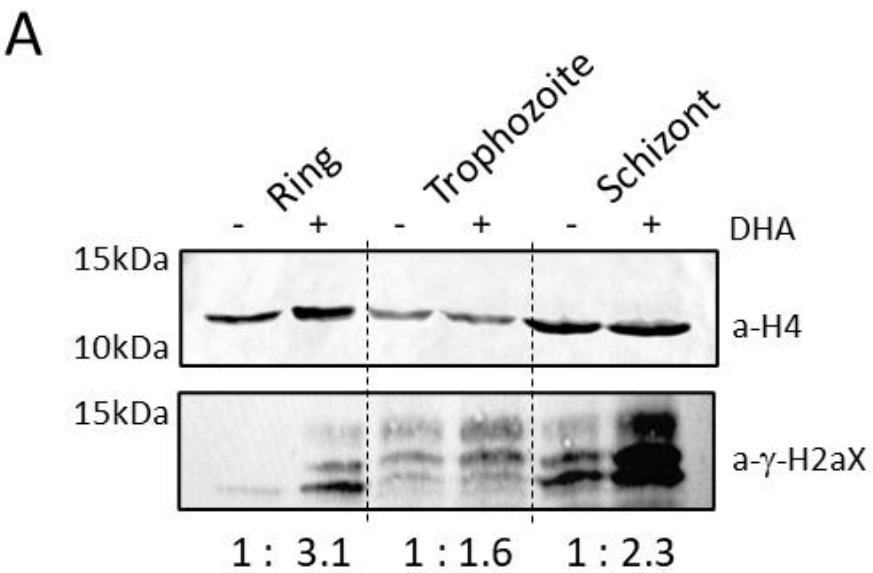
A
Ring
Trophozoite
Schizont
- + - + - +
DHA
15kDa
10kDa
a-H4
15kDa
a-γ-H2aX
1 : 3.1
1 : 1.6
1 : 2.3

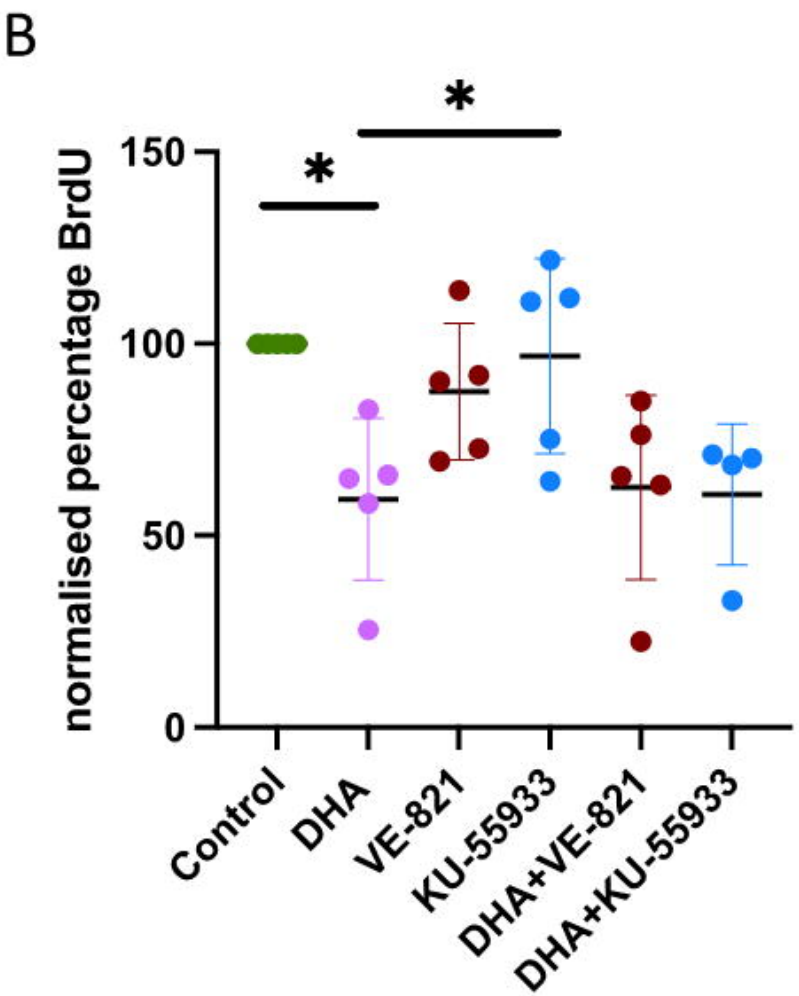
B
normalised percentage BrdU
150
100
50
0
*
*
Control
DHA
VE-821
KU-55933
DHA+VE-821
DHA+KU-55933

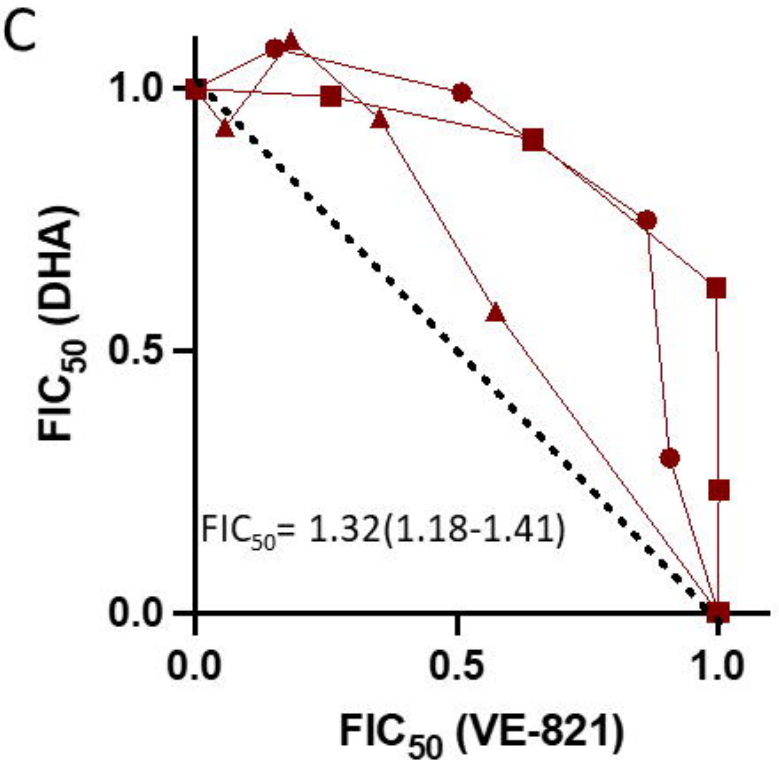
C
FIC50 (DHA)
1.0
0.5
0.0
FIC50= 1.32(1.18-1.41)
0.0
0.5
1.0
FIC50 (VE-821)

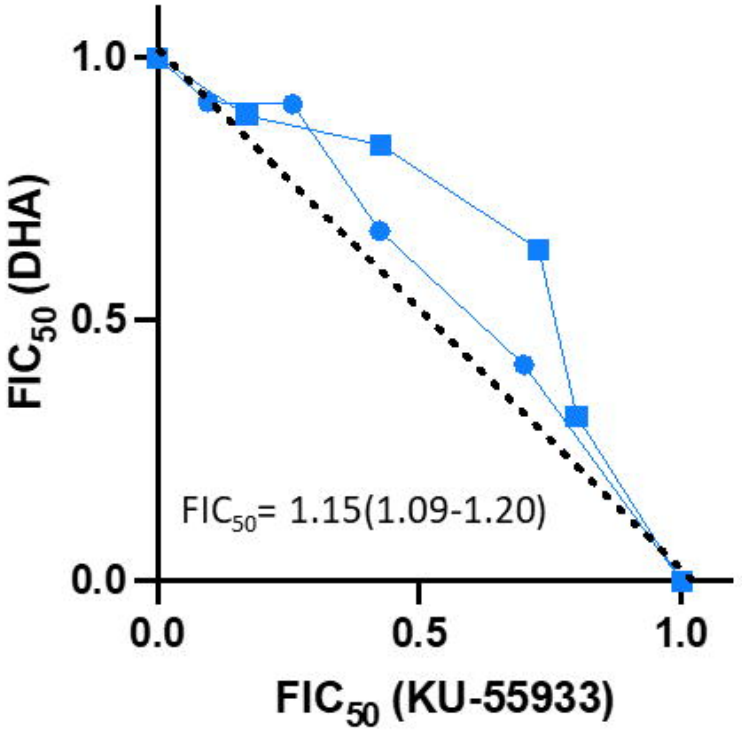
FIC50 (DHA)
1.0
0.5
0.0
FIC50= 1.15(1.09-1.20)
0.0
0.5
1.0
FIC50 (KU-55933)

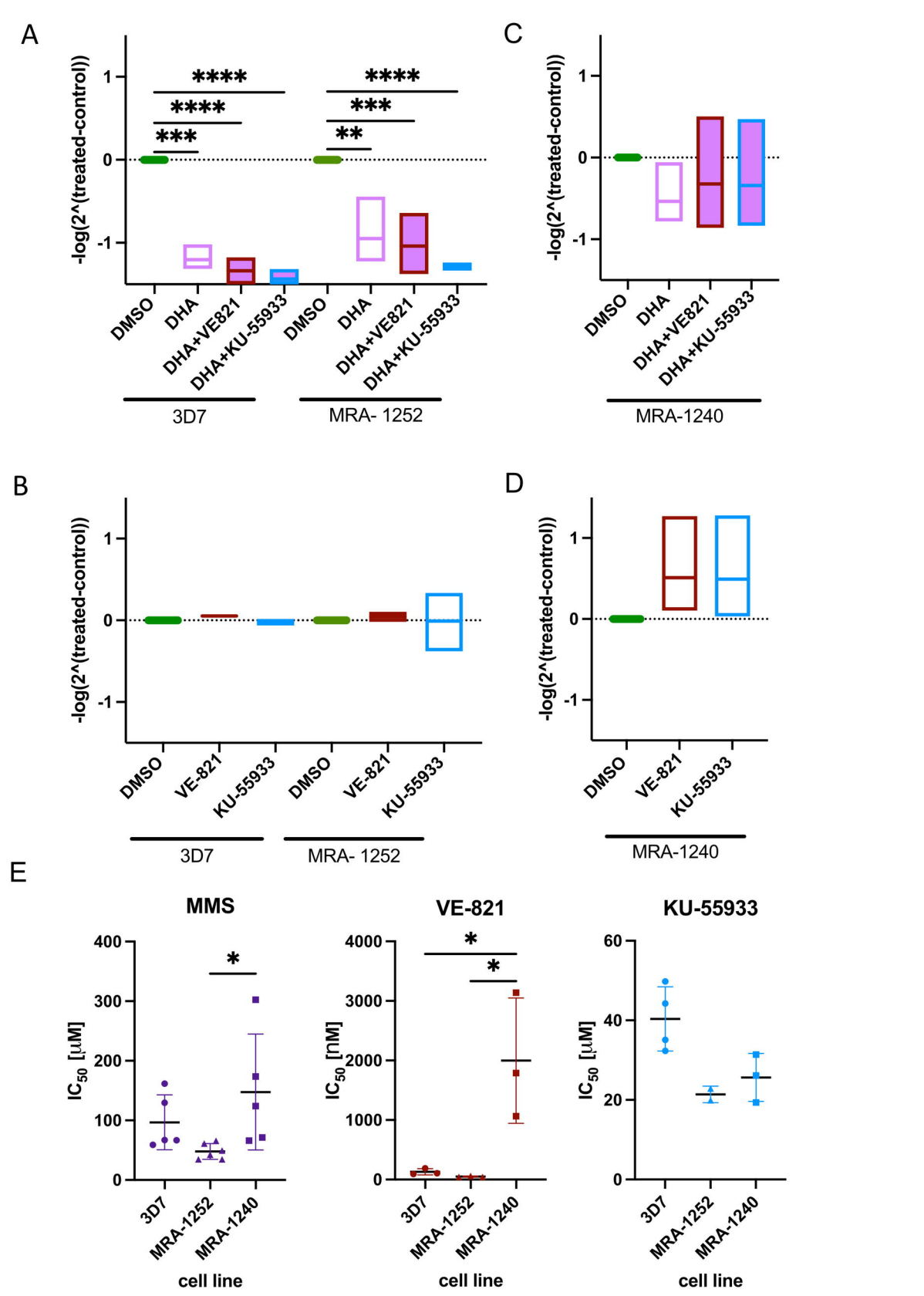
A
-log(2^(treated-control))
1
0
-1
****
****
***
****
***
**
DMSO
DHA
DHA+VE821
DHA+KU-55933
DMSO
DHA
DHA+VE821
DHA+KU-55933
3D7
MRA- 1252
C
-log(2^(treated-control))
1
0
-1
DMSO
DHA
DHA+VE821
DHA+KU-55933
MRA-1240
B
-log(2^(treated-control))
1
0
-1
DMSO
VE-821
KU-55933
DMSO
VE-821
KU-55933
3D7
MRA- 1252
D
-log(2^(treated-control))
1
0
-1
DMSO
VE-821
KU-55933
MRA-1240
E
MMS
IC50 [µM]
400
300
200
100
0
*
3D7
MRA-1252
MRA-1240
cell line
VE-821
IC50 [nM]
4000
3000
2000
1000
0
*
*
3D7
MRA-1252
MRA-1240
cell line
KU-55933
IC50 [µM]
60
40
20
0
3D7
MRA-1252
MRA-1240
cell line